Stratigraphic controls on a salt-withdrawal intraslope minibasin, north-central Green Canyon, Gulf of Mexico: Implications for misinterpreting sea level change

Andrew S. Madof, Nicholas Christie-Blick, and Mark H. Anders

ABSTRACT

Three-dimensional seismic data from the Fuji basin, a salt-controlled intraslope minibasin in north-central Green Canyon, Gulf of Mexico, reveal complex interactions between gravity- and suspension-driven sedimentation. Seismic volumes for late Pleistocene (~470 ka) to Holocene fill within the Fuji basin consist of approximately 45% mass transport complexes (MTCs), 5% channelized sandy turbidites, and 50% hemipelagites and muddy turbidites. At least ten MTCs within the Fuji basin flowed radially toward its depocenter, either from basin flanks (i.e., intrabasinal) or as a result of larger-scale salt motion (i.e., extrabasinal). Sediment transport directions are inferred on the basis of elongate basal incisions and smaller-scale scours, head scarps, fold orientation within the complexes, and stratigraphic thinning trends at downdip margins. An amalgamated set of three channelized sandy turbidite complexes less than 350 m (1148 ft) thick and 3 km (1.8 mi) across represents the main sand delivery pathway into the Fuji basin. These deposits are thought to be due to shelf bypass, and possibly, to proximity to the Pleistocene shoreline. Hemipelagites and muddy turbidites are homogeneous, and their thickness is relatively consistent at basin scale. This facies represents background sedimentation.

Manuscript received June 16, 2008; provisional acceptance August 5, 2008; revised manuscript received October 31, 2008; final acceptance December 22, 2008.
DOI:10.1306/12220808082

AUTHORS

ANDREW S. MADOF ~ *Department of Earth and Environmental Sciences and Lamont-Doherty Earth Observatory of Columbia University, Palisades, New York 10964; amadof@ldeo.columbia.edu*

Andrew S. Madof is a Ph.D. candidate at Columbia University's Lamont-Doherty Earth Observatory. He received his B.A. degree from Oberlin College in 2000, his M.S. degree from the University of Kansas in 2006, and his M.Phil. degree from Columbia University in 2008. His research focuses on the noneustatic controls on both shallow-marine and deep-water systems and particularly on the role of deformation in modulating accommodation.

NICHOLAS CHRISTIE-BLICK ~ *Department of Earth and Environmental Sciences and Lamont-Doherty Earth Observatory of Columbia University, Palisades, New York 10964*

Nicholas Christie-Blick is a professor of earth and environmental sciences at Columbia University's Lamont-Doherty Earth Observatory. He completed his Ph.D. at the University of California, Santa Barbara, in 1979, and was a research scientist at Exxon Production Research Company in Houston for three years in the early 1980s. Christie-Blick's research and publications deal with such varied topics as sedimentation processes, crustal deformation, and deep-time Earth history, with emphasis on challenging conventional thinking and resolving outstanding disagreements.

MARK H. ANDERS ~ *Department of Earth and Environmental Sciences and Lamont-Doherty Earth Observatory of Columbia University, Palisades, New York 10964*

Mark H. Anders is an associate professor of earth and environmental sciences at Columbia University's Lamont-Doherty Earth Observatory. He received his Ph.D. from the University of California at Berkeley in 1989 working with Walter Alvarez, and joined the Columbia faculty that year. He and his students work on a wide range of topics related to faults and the faulting process, including fault growth, the effects of magmatism on extension, and more recently, the mechanics of large block slides.

ACKNOWLEDGEMENTS

The authors acknowledge Chevron for summer internships (Madof) and for access to proprietary biostratigraphic data, Compagnie Générale de Géophysique-Veritas for the loan of 3-D seismic reflection data, Paradigm for providing access to VoxelGeo commercial interpretation software, and National Science Foundation grant OCE 01-19019 for the recent support of our sequence-stratigraphic studies (Christie-Blick). We are especially grateful to Jason R. Cansler, Tom L. Elliott, Barney Issen, David C. Lentrichia, Ivan D. Marroquin, Martin A. Perlmutter, Serge Sauvagnac, Luc Schlumberger, and Nat G. Smith for making it possible to undertake this project. We thank Frank D. Bilotti, Walter C. Pitman III, William B.F. Ryan, Michael S. Steckler, and Charles Stelting for engaging discussions about the emerging interpretation, and Janok P. Bhattacharya, D. Bradford Macurda Jr., Zoltan Sylvester, and AAPG editor Gretchen Gillis for helpful reviews. Lamont-Doherty Earth Observatory contribution number 7215.

A process-driven model has been developed involving halokinetic autocyclicity as the primary control on sedimentation in the Fuji basin. Passive salt motion accounts better for both the directions of sediment transport and the frequency of late Pleistocene–Holocene MTCs than currently popular eustatic and steady-state bathymetric models. The conclusion is significant in casting doubt on the generally assumed importance of eustasy in controlling off-shelf lowstand sedimentation and in implying marked variations in stratigraphic details at length scales of less than 10 km (6.2 mi).

INTRODUCTION

Conventional wisdom suggests that sedimentation in intraslope deep-water depositional systems is governed by either eustasy or steady-state bathymetry. The eustatic model asserts a correlation between sea level and facies assemblages (Weimer, 1990; Posamentier and Kolla, 2003), where sediment is derived primarily from the shelf and at time scales that relate to the frequency of eustatic cycles. The bathymetric model proposes an association between antecedent physiography in salt-withdrawal minibasins and instantaneous patterns of sedimentation (Prather et al., 1998; Winker and Booth, 2000).

According to the eustatic model, at high stands of sea level, deposition of coarse-grained sediments occurs preferentially in shallow-marine environments. Deep-water settings are characterized mainly by background (hemipelagic) sedimentation. At falls in sea level, low permeability leads to an increase in pore-fluid pressure relative to the ambient confining pressure. Overpressure produced in this way contributes to slope failure and the initiation of mass transport complexes (MTCs), which are for this reason widely regarded as proxies for falling sea level in deep-water regimes (Weimer, 1990; Posamentier and Kolla, 2003). At eustatic low stands, sediment delivered to the slope is thought to bypass the shelf via incised valleys. Subsequent rapid rises of sea level can produce slope instabilities through water and sediment loading, which in some cases may lead to a second generation of MTCs (Posamentier and Kolla, 2003).

According to the bathymetric model, coarse-grained sediment is able to pond at depths greater than basin spill points but is assumed to bypass whenever basins become overfilled (Winker and Booth, 2000; Mallarino et al., 2006). The preservation potential of such sediment can therefore be inferred from a comparison of local slope profiles with regional profiles. Hemipelagic sediments drape the bathymetry, and their distribution is not influenced by such considerations.

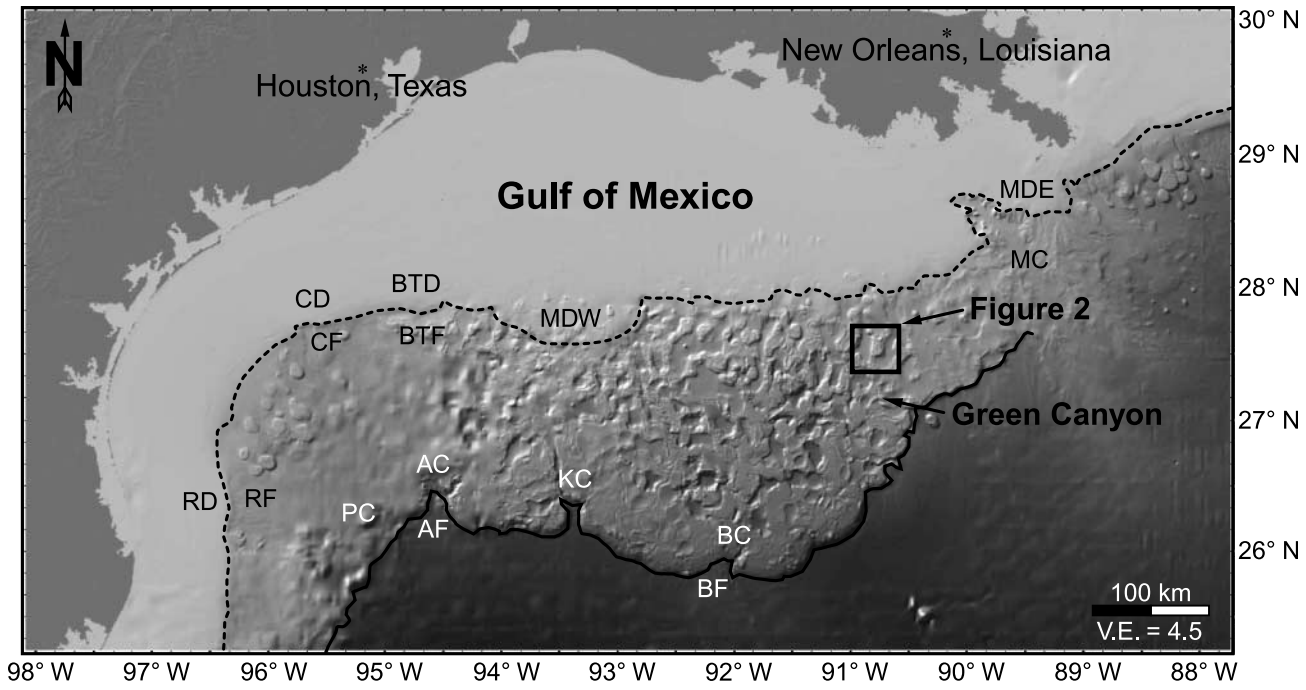

Figure 1. Bathymetric map of Gulf of Mexico (created using GeoMapApp; Marine Geoscience Data System, 2008) (see Carbotte et al., 2004), showing Pleistocene paleogeographic features and rugose bathymetry associated with shallow salt emplacement. Dashed line delineates approximate boundary between modern shelf (north) and slope (south). Solid line outlines the Sigsbee Escarpment. Abbreviations for Pleistocene features (from Winker and Booth, 2000) are as follows. Shelf margin deltas: RD = Rio Grande; CD = Colorado; BTD = Brazos-Trinity; MDW = Mississippi western; MDE = Mississippi eastern; submarine canyons: PC = Perdido; AC = Alaminos; KC = Keathley; BC = Bryant; MC = Mississippi; submarine fans: RF = Rio Grande; CF = Colorado; BTF = Brazos-Trinity; AF = Alaminos; BF = Bryant; V.E. = Vertical exaggeration.

This study makes use of commercial three-dimensional (3-D) seismic reflection data from the Fuji basin, a salt-withdrawal intraslope minibasin located in north-central Green Canyon, Gulf of Mexico, to evaluate these competing ideas. Little has been published on the Fuji basin (Acosta, 1994; McBride, 1997; Soto, 1997) because of the proprietary nature of much of the seismic-reflection and well data. The present study provides the first publicly available 3-D interpretation of seismic facies and architecture for the basin.

STRATIGRAPHIC AND TECTONIC SETTING

The Fuji basin, an upper Pliocene to Holocene salt-withdrawal structure associated with sediment loading (McBride, 1997), is located within the Middle Jurassic to Holocene-aged Gulf of Mexico passive margin (Figures 1, 2). The basin is part of a much broader province of salt-withdrawal intraslope minibasins with comparable physiography. The Fuji basin is approximately 30 km (18.6 mi) long and 15 km (9.3 mi) wide and oriented north–south. The floor of the basin is currently 1.3 km (4200 ft) below the sea surface and as much as 0.5 km (1700 ft) below the crests of flanking salt-cored highs. The northern margin is delineated by the Nagano fault, a growth fault related to salt withdrawal (McBride, 1997).

The Gulf of Mexico passive margin formed as a result of the breakup of Pangea (Buffler and Sawyer, 1985; Salvador, 1987, 1991; Feng et al., 1994; Bird et al., 2005). The Gulf is underlain primarily by oceanic crust and rimmed by transitional to continental crust (Bird et al., 2005). During the Middle to Late Jurassic, up to several kilometers of salt were deposited as a result of the evaporation of sea water in restricted embayments (Diegel et al., 1995). The accumulation of thick Mesozoic and Cenozoic sediments subsequently mobilized the salt, which became generally allochthonous during

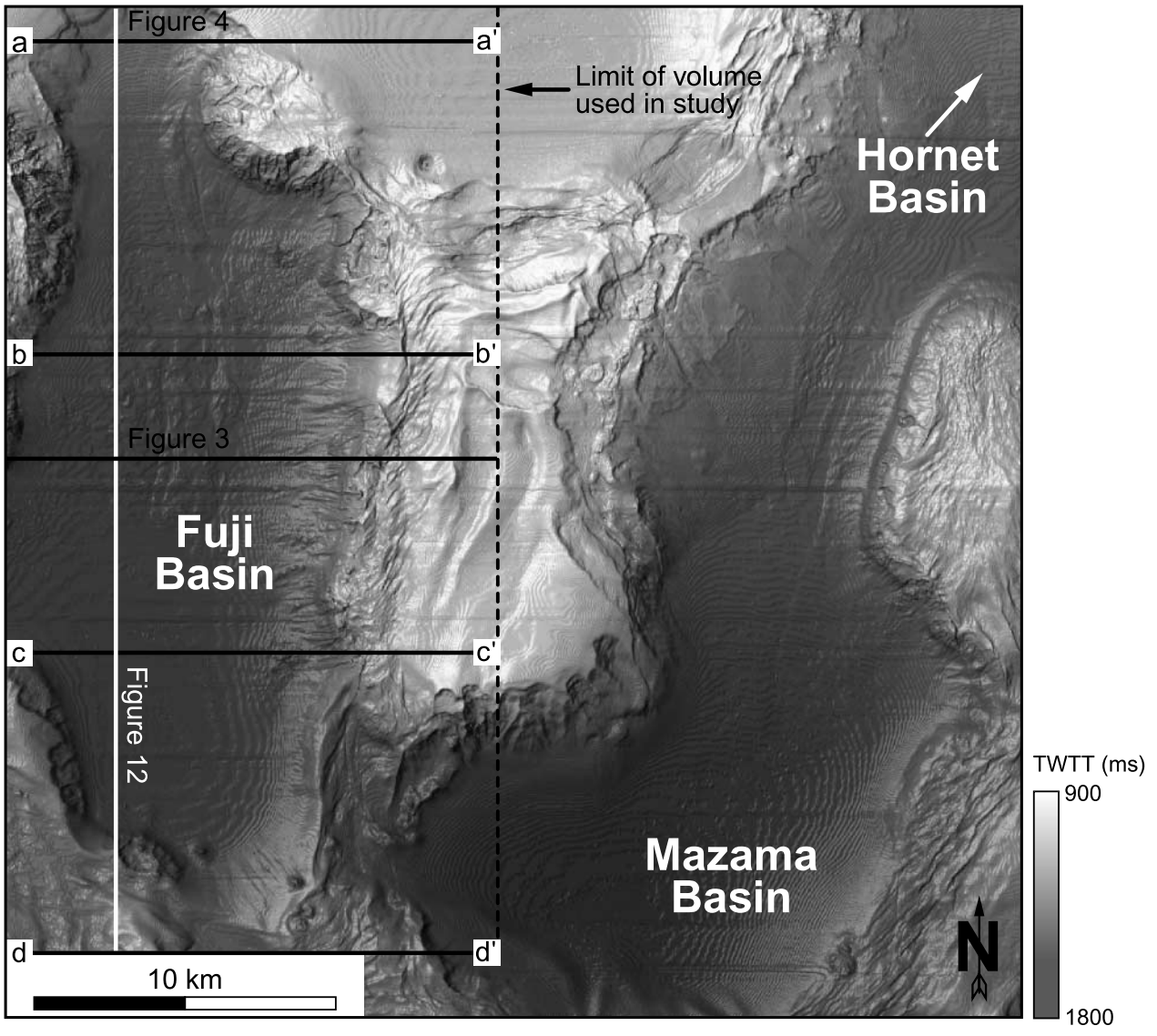

Figure 2. Bathymetric map of Fuji, Mazama, and Hornet basins (dark gray), separated by salt-controlled structural high (white). Note the dimensions of the volume used in this study and the orientations of Figures 3, 4aa′–dd′, and 12. TWTT = two-way traveltime.

the Oligocene to Miocene (Diegel et al., 1995). Contemporary progradation and loading by deep-water sediments (Prather et al., 1998) are responsible for the present-day rugose bathymetry.

Sedimentation above a mobile salt substrate has been the primary control on the stratigraphic evolution of the Gulf of Mexico since the Miocene. At that time, the Mississippi River depocenter was located in the eastern Gulf. Sediment overfilled shallow bathymetric depressions (minibasins), inducing bypass to the abyssal plain (Winker and Booth, 2000). By the late Pliocene to early Pleistocene, the depocenter had migrated westward as a result of the reorganization of the Mississippi River drainage (Prather et al., 1998; Winker and Booth, 2000). Intraslope minibasins became well developed during the late Pleistocene, with bypass via submarine canyons to the Mississippi Fan and, to a lesser degree, the Bryant and Alaminos fans (Winker and Booth, 2000).

In the vicinity of the Fuji basin, pre-Pliocene stratigraphy consists primarily of deep-water deposits influenced by shallow (allochthonous) salt mobility. More than 6.0 km (20,000 ft) of deep-water sediment accumulated in the Fuji basin during the Pliocene and Pleistocene (Soto, 1997). McBride

(1997) showed that the salt canopy was fed from a deeper salt source until 3.8 Ma, when that source became exhausted. The flow of shallow salt to the east, west, and south is responsible for the modern bathymetry. Salt was completely evacuated from beneath the Fuji basin by 0.2 Ma, permitting the minibasin fill to rest directly on subsalt stratigraphy and form a salt weld within the Pliocene some 7.6 km (25,000 ft) below sea level.

DATA AND METHODOLOGY

The 3-D seismic reflection data used for this study cover 18 blocks of the outer continental shelf (Figure 2) and encompass an area of 420 km^2 (162 mi^2) to a depth of 4000 ms (1.8 km/5900 ft). The data were acquired during 1999–2000 and reprocessed in 2001 using a modeled signature to approximate zero phase. Prestack time-migrated volume has a frequency of 50–60 Hz and a bin spacing of 20 × 12.5 m (66 × 41 ft), with a vertical sampling rate of 4 ms. The vertical resolution of the data is approximately 10 ms (7.5 m/25 ft). Sediment velocities were estimated to be roughly 1500 m/s based on previous studies in the Gulf of Mexico (Winn et al., 1998; Bevc et al., 2003; McDonnell et al., 2008). This figure is used for all depths in the Fuji basin because a velocity model is not available.

Nineteen seismic surfaces (Figure 3) were picked and used to interpret the Fuji basin's stratigraphy at high resolution and in three dimensions. Surfaces were chosen for both stratigraphic and practical reasons, for example, where high-amplitude reflections are present directly above or below chaotic intervals and at other levels characterized by lateral continuity. Each surface is associated with a characteristic amplitude: peak, trough, or zero crossing (a change from peak to trough or vice versa). After a reflection was selected, the 3-D propagator algorithm was used to cross-correlate nearest-neighbor seismic traces to within a defined confidence interval. This workflow created 3-D seismic surfaces, which were subsequently inspected by panning through each trace for every surface. Where the propagator algorithm miscorrelated, surfaces were manually adjusted to the correct reflection.

Discontinuities arise within reflections as artifacts of the propagator algorithm (e.g., where reflection amplitude is less than the predetermined threshold), and as a result of reflection geometry (e.g., where reflecting interfaces are too steep, and where one reflection terminates against another by baselap, truncation, stratigraphic thinning or faulting). Locally steep interfaces associated with rugose bathymetry are particularly problematic in the Fuji basin. Physical surfaces, therefore, are more continuous than might be inferred from initial use of the propagator (e.g., seismic surface no. 15, Figure 3B).

FACIES ASSEMBLAGES

Three seismic facies assemblages compose the basin fill above 4000 ms (Figure 4): the MTC facies (~45% of the total), the channelized sandy turbidite facies (~5%), and the hemipelagite and muddy turbidite facies (~50%). Facies assemblages are identified and delineated on the basis of amplitude, cross-sectional continuity, internal architecture, external form, and lower bounding surfaces (Table 1). Interpretations of lithology are based solely on these criteria, as the authors did not have access to proprietary well data and core in the study area. However, the authors were granted access to biostratigraphic data (discussed in the Age Control section).

The MTCs are characterized by hummocky to mounded, high- to low-amplitude reflections. These deposits, which vary greatly in both expression and volume of individual units, are found preferentially in the depocenter of the Fuji basin, becoming more abundant and increasingly amalgamated up section. Channelized sandy turbidites, the least voluminous assemblage, are identified on the basis of low cross-sectional continuity and high-amplitude reflections. This assemblage is characterized by relatively low spatial variability, and it continues to the south and southeast beyond the edge of the seismic volume. Hemipelagite and muddy turbidites, the most voluminous assemblage,

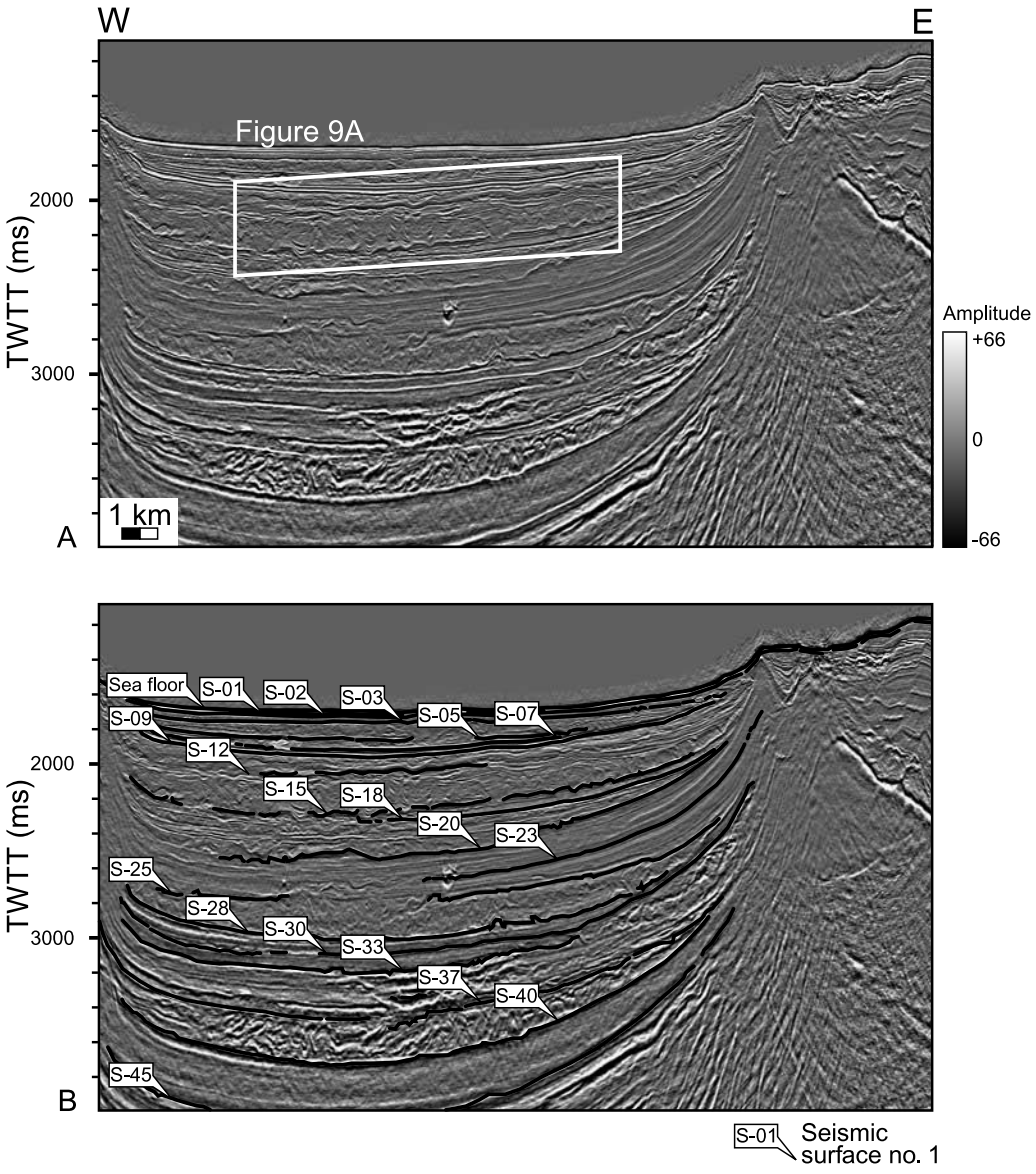

Figure 3. East-west–oriented seismic profile: (A) uninterpreted and (B) interpreted. Interpreted profile shows 19 picked seismic surfaces: S-01 denotes seismic surface no. 1. The scale is the same in both panels. See Figure 2 for the orientation of profile. TWTT = two-way traveltime.

correspond with low-amplitude reflections of relatively nondescript and homogeneous character and with intervals of roughly uniform thickness.

MTCs: Observations

The MTCs constitute the most variable assemblage and consist of hummocky, mounded, and chaotic, high- to low-amplitude reflections, exhibiting a wedge-shaped or lenticular external form (Table 1). Units have an erosional, scoured, or low-angle basal surface. The facies is characterized by high to moderate cross-sectional continuity, with a locally folded or faulted internal architecture.

Units composing the MTC facies range in thickness from less than 50 ms (~65 m [213 ft]) to more than 200 ms (~265 m [869 ft]) and in area from a few square kilometers to more than 300 km^2 (116 mi^2). Individual deposits thin toward the basin margins and decrease in volume and areal extent up section.

The MTCs exhibit a wide variety of basal erosional features (Figure 5A–C). Of these, the two most common are large-scale basal incision and small-scale scour, which remove from more than 50 km^2 (19 mi^2) to less than 1 km^2 (0.3 mi^2), respectively, of the underlying deposits. Basal incision exhibits up to 100 ms (~133 m [436 ft]) of relief, whereas scours have maximum dimensions

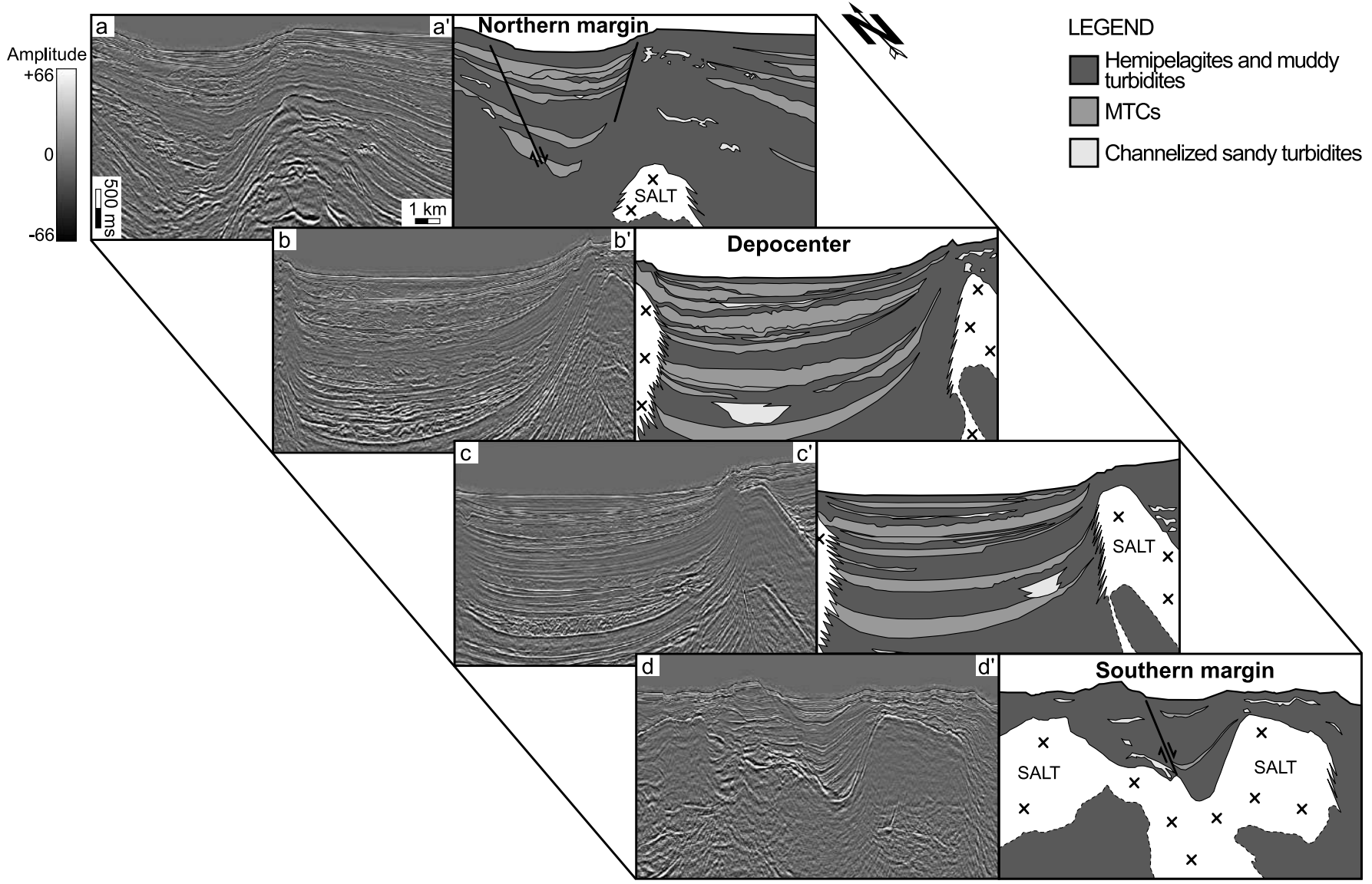

Figure 4. Gross stratigraphic architecture of the Fuji basin composed of approximately 45% mass transport complexes (MTCs), 5% channelized sandy turbidites, and 50% hemipelagites and muddy turbidites. See Figure 2 for the location of seismic profiles.

Table 1. Summary of Seismic Character for Three Facies Assemblages

	Amplitude	Cross-Sectional Continuity	Internal Architecture	External Form	Lower Bounding Surface
Mass transport facies assemblage	High to low/ transparent	High to moderate	Hummocky, mounded, and chaotic	Wedged or lenticular	Erosional, scoured, or low angle
Channelized sandy turbidite facies assemblage	High	Low	Concave, lenticular, or tabular	Ribbon shaped	Erosional or low angle
Hemipelagite and muddy turbidite facies assemblage	High to low/ transparent	High	Planar and parallel	Wedged, lenticular, or tabular	Planar

of 10 km (6.2 mi) (length) × 2 km (1.2 mi) (width) × 50 ms (~65 m [213 ft]) (depth). The width and depth of erosional relief in both cases decrease downdip, terminating abruptly.

In the absence of such relief, MTCs are underlain by gently inclined high-amplitude reflections. In one instance (Figure 5B), a planar basal discontinuity passes downdip (to the northwest) across a step into an irregular surface with up to 50 ms (~65 m [213 ft]) of relief. The hummocky character of the deposits increases abruptly across the same feature.

Folds are found on a variety of scales within MTCs in the study area (Figures 5A, B, D; 6; 7). In the most noteworthy and seismically well-preserved example (Figures 5D, 6), northeast-trending folds occupy an area of 30 km^2 (11 mi^2). Wavelengths range from 100 to 500 m (328 to 1640 ft), and amplitudes from 20 ms (~25 m [82 ft]) to 50 ms (~65 m [213 ft]), in both cases decreasing toward the north.

Internal faults are locally associated with folds (Figure 6). In the example illustrated, reverse faulting accommodates from 0.8 to 1.3 km (0.4 to 0.8 mi) of shortening, based on measurements of fault heave. The direction of shortening is oblique to the overall orientation of the MTC.

MTCS: Interpretations

At least 10 MTCs are interpreted in the Fuji basin. Of these, intrabasinal MTCs are confined within the basin. Extrabasinal MTCs, present near the base of the interpreted volume, are thicker and more laterally persistent and spill outside the basin margins.

The MTC assemblage is interpreted to represent a spectrum of gravity-driven phenomena (Figure 8). Although the subdivision of MTCs into slides, slumps, debris slides, and debris flows can be made at the scale of outcrop and core, they are commonly below the resolution of seismic data (McHugh et al., 2002). For this reason, sediment failure deposits have all been grouped into the MTC facies assemblage.

The lithology of MTCs depends primarily on the sediments from which they are derived. The MTCs characterized by low-amplitude reflections are interpreted to be composed of uniform relatively fine-grained deposits. Units with both high and low amplitudes are inferred to be heterolithic (muddy sediments interbedded with coarse-grained or sandy deposits). In the absence of well control, these interpretations are necessarily tentative. An MTC that was interpreted on the basis of seismic reflection data at a nearby location, and subsequently cored and logged by the Integrated Ocean Drilling Program, proved to consist of unconfined and undeformed sandy turbidite sheets interstratified with mud (Expedition 308 Scientists, 2005).

The MTCs are nevertheless well documented worldwide and in both passive and active continental margin settings (Nissen et al., 1999; Beaubouef and Friedmann, 2000; McHugh et al., 2002; Haflidason et al., 2004; Bünz et al., 2005; Gee et al., 2005; Martinez et al., 2005; Moscardelli et al., 2006). Among general conclusions from these studies, transport and deposition are influenced by preexisting topography, slides and flows are cohesive but commonly entrain water while active, and consolidation occurs shortly after deposition (McHugh et al., 2002; Posamentier and Kolla, 2003; Moscardelli et al., 2006). The leading edge is shortened

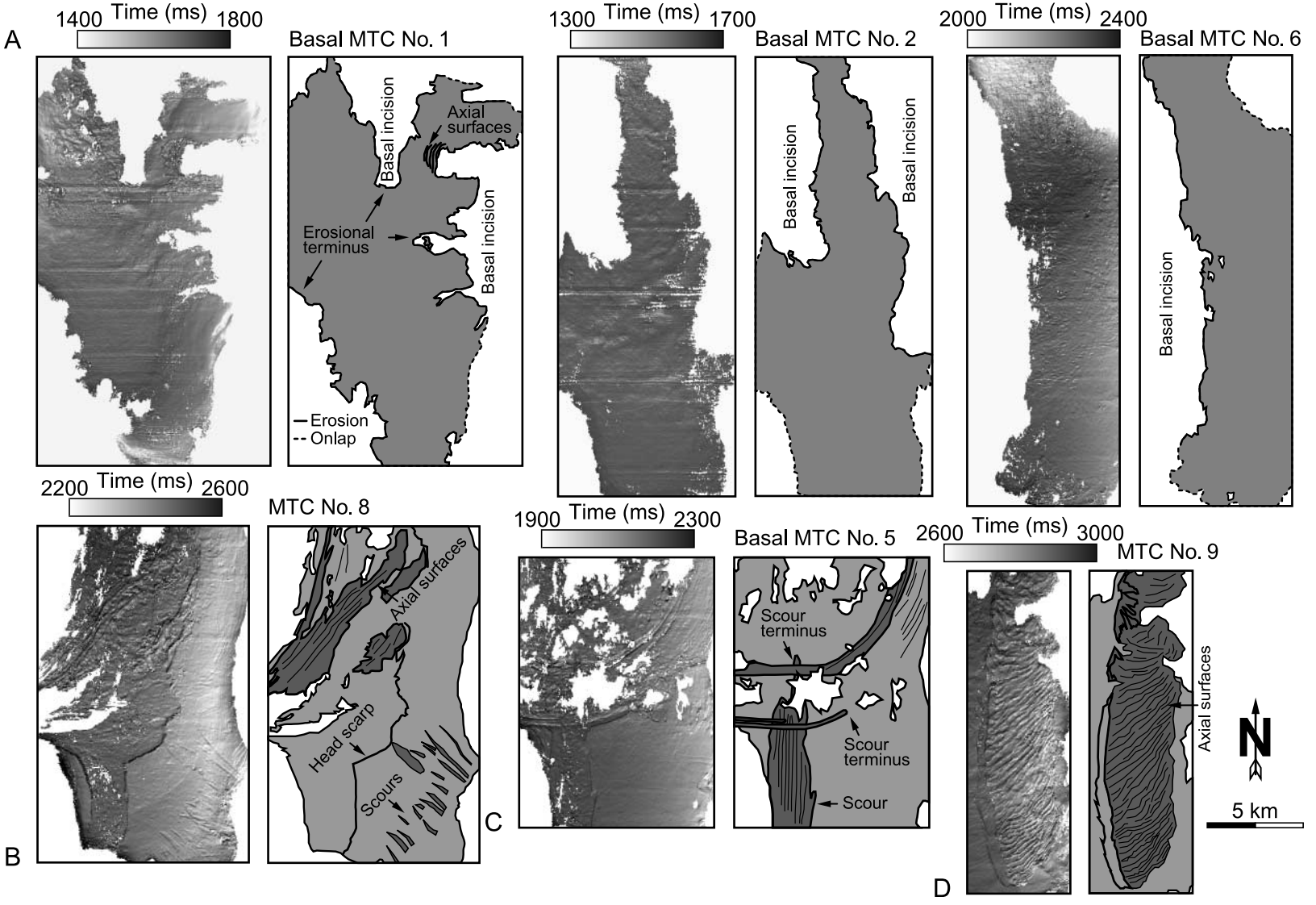

Figure 5. Uninterpreted and interpreted features associated with mass transport complex (MTC) facies assemblage. Scale and north are the same in all panels. (A) Three time horizons showing planar basal detachments and erosional truncation of the underlying deposits. (B) The MTC no. 8 showing head scarp, traces of axial surfaces, and scours. Scours in the southeastern part of the surface are from preexisting deposit. (C) Intersecting scours showing superimposed deposits. (D) Traces of axial surfaces. The greatest amplitudes and shortest wavelengths are associated with folds in the south.

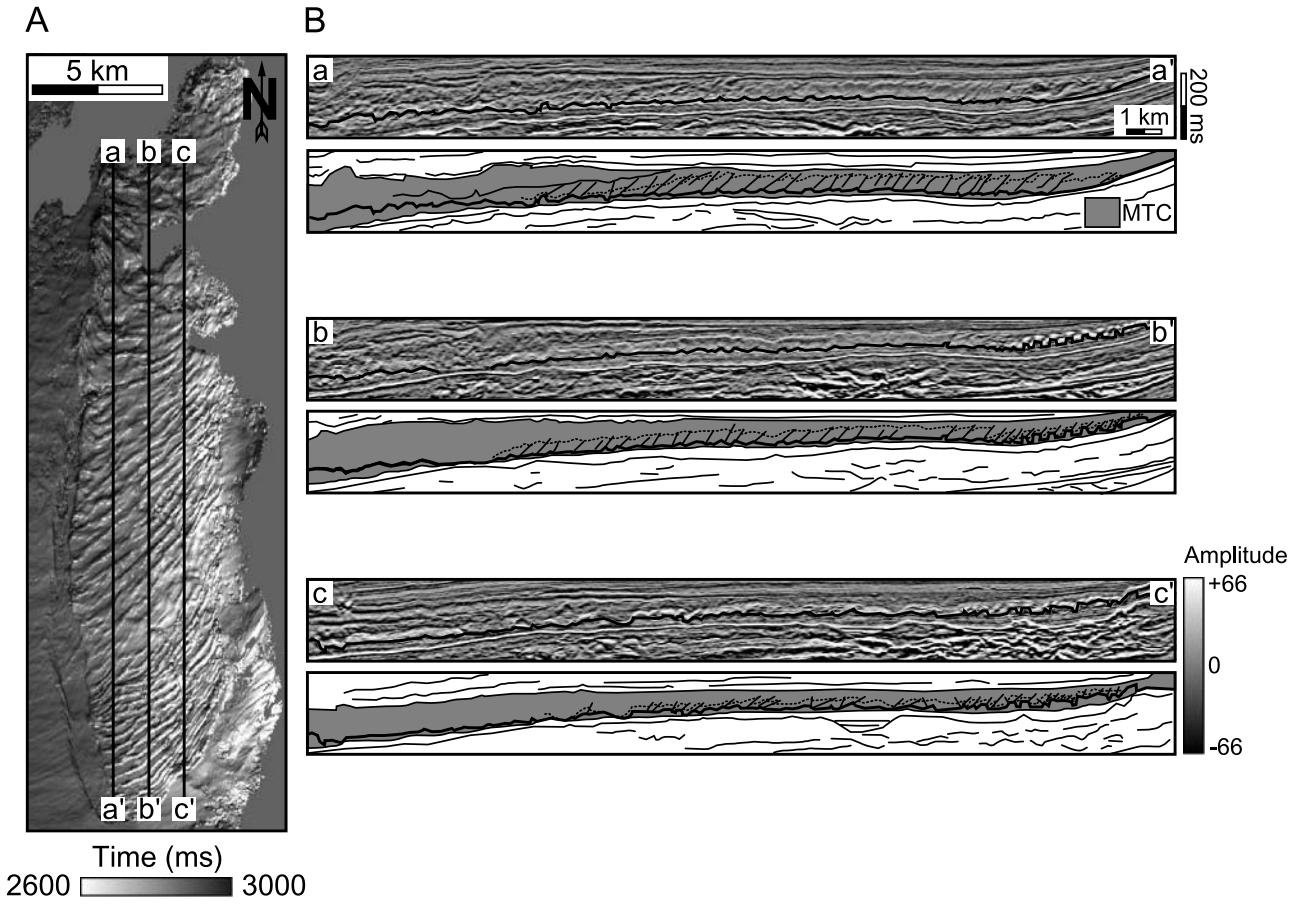

Figure 6. Differential shortening within MTC facies. (A) Folded surface from Figure 5D, located above the base of MTC no. 9. Note the location of three seismic profiles. (B) Three uninterpreted and interpreted profiles showing internal folding and faulting. In the west (aa'), 1.3 km (0.8 mi) of shortening is accommodated on numerous faults, which almost vertically penetrate the deposit. In the east (cc'), 0.8 km (0.4 mi) of shortening is accommodated on fewer faults concentrated toward the base of the unit. Shortening was estimated from fault heaves. Note the eastward thinning of the deposit.

and thickened during transport, with the development of syndepositional thrusts, folds, and chaotic structure. The trailing edge is extended and thinned, associated with listric normal faults and tilted blocks, and bounded by a head scarp (Martinez et al., 2005). Lateral margins are commonly characterized by detached transfer faults.

Incision accompanies downslope motion, with the incorporation of underlying material into the evolving complex, and continues until materials become disaggregated or they begin to hydroplane at a break in slope (Posamentier and Kolla, 2003). Erosion occurs under both confined and unconfined conditions. Confined flow is commonly identified by parallel or converging scour marks, whereas unconfined flow is interpreted by diverging tracks. The depth of incision is greatest beneath the thickest parts of the deposit and decreases toward downdip and lateral margins.

Channelized Sandy Turbidites: Observations

The channelized sandy turbidite facies is characterized by high-amplitude reflections, consisting of concave, lenticular, or tabular internal elements and exhibiting a ribbon-shaped external form. The facies assemblage commonly overlies an erosional or low-angle basal surface and is associated with low cross-sectional continuity (Table 1).

The hierarchy of depositional elements constituting the channelized sandy turbidites consists of

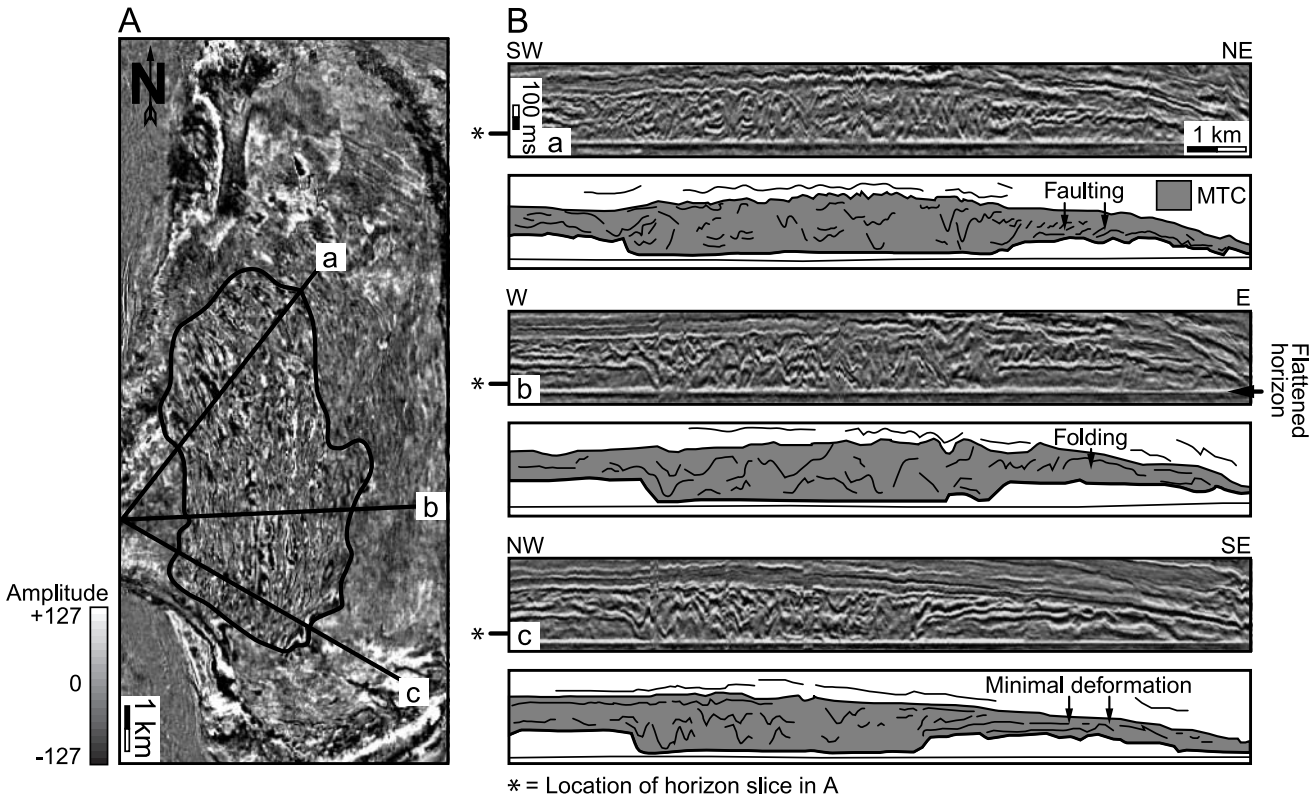

Figure 7. The MTC no. 10 showing the internal disorganization of the deposit. (A) Horizon slice (plan view) showing radially oriented axial surfaces, delineated by a black polygon. (B) Three seismic profiles oriented perpendicular to the trace of axial surfaces, showing the internal structure. Note the lateral change from faulting (northeast) to minimal deformation (southeast).

meandering ribbon-shaped channels (Figure 9), laterally and vertically arranged into channel complexes (Figure 10). These complexes are floored by a master erosional surface and capped by a planar upper boundary.

The individual channel is the most fundamental unit of the facies, with dimensions of more than 30 km (18.6 mi) (length) × 0.1 km (0.06 mi) (width) × 25 ms (~33 m [108 ft]) (depth). Channels exhibit high to moderate sinuosity and increase in length and lateral expansion (i.e., swing) up section. In one example, levees appear to be present at the southern end of a channel (Figure 11B). Levees, lateral accretion, and down-system meander-loop migration (i.e., sweep) are otherwise not readily observed in channels within the study area.

Channel complexes comprise variably stacked, laterally and vertically amalgamated channels. Complexes have a bypass character with dimensions of greater than 30 km (18.6 mi) (length) × 1.5 km (0.9 mi) (width) and are floored by a master erosional surface displaying up to 200 ms (~266 m [873 ft]) of relief (Figure 10). None of these deposits displays a distributary morphology. Complexes, as with component channels, increase in length and lateral expansion up section, and they are oriented north–south to northwest–southeast (Figure 11). Sediment transport directions for these deposits are assumed to be southward. The largest unit of this facies, illustrated in Figures 10 and 11, consists of a single example of a set of channel complexes, with dimensions exceeding 30 km (18.6 mi) (length) × 3 km (1.8 mi) (width) × 250 ms (~333 m [1092 ft]) (depth). Taken together, this interval displays an up-section increase in length, swing, and width.

Channelized Sandy Turbidites: Interpretations

Gravity-driven channelized sandy turbidites (Figure 8) are conventionally identified on the basis of their high-amplitude character, lack of cross-sectional

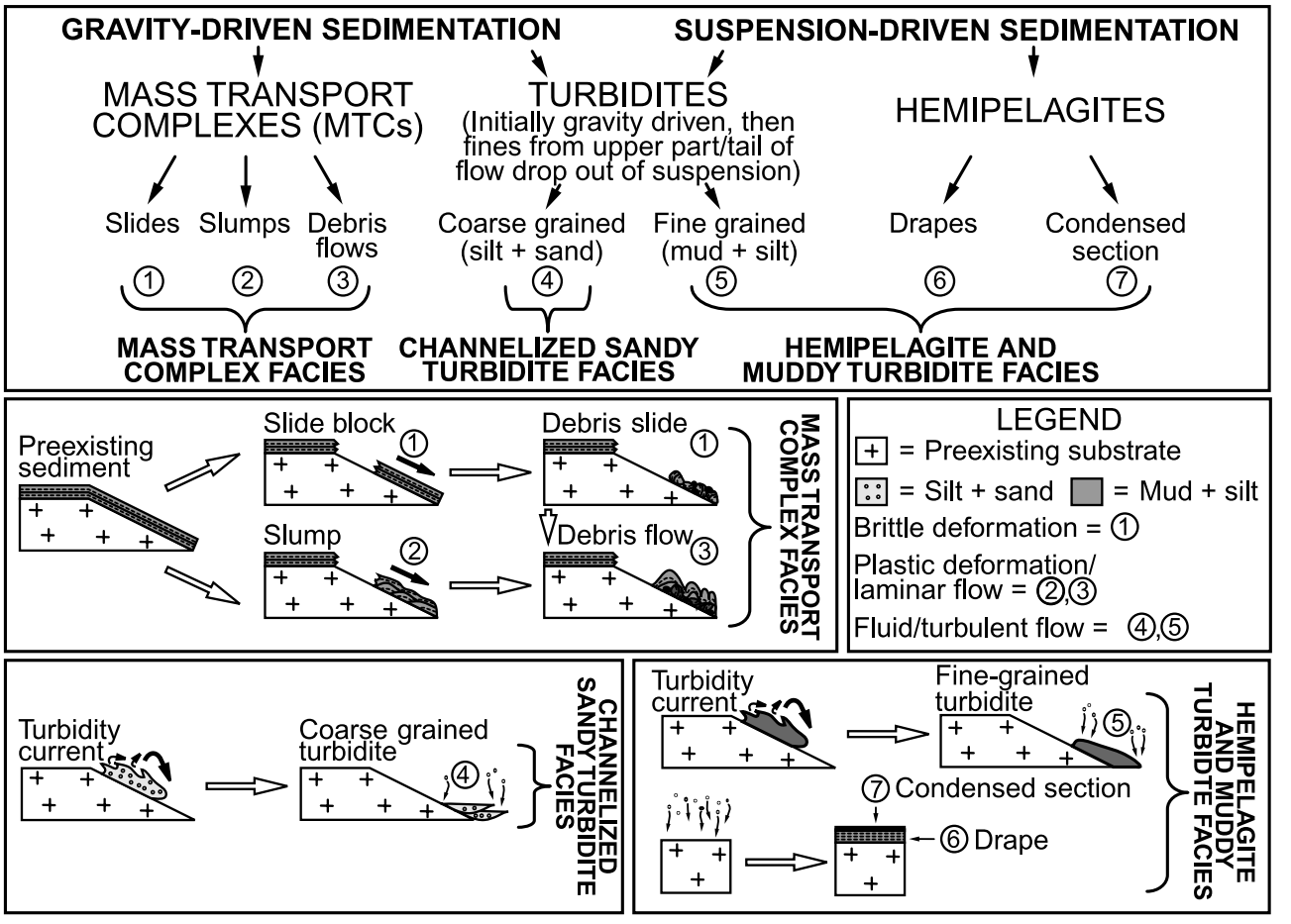

Figure 8. Summary of processes responsible for the deposition of seismic facies assemblages (modified from McHugh et al., 2002).

continuity, and ribbon-shaped plan-view morphology (Weimer, 1990; Peakall et al., 2000a, b; Posamentier and Kolla, 2003). Without lithologic calibration to seismic data, this interpretation cannot be substantiated but is reasonable based on the external morphology and internal structure of the facies.

Bend development within channelized sandy turbidites has been interpreted to evolve from relatively straight to meandering (Peakall et al., 2000a, b). As channelized sandy turbidity currents flow downslope, swing is constrained by channel inflection points (i.e., stationary bend nodes). Over time, the length, sinuosity, and depth of the channel increase, whereas the wavelength decreases (Peakall et al., 2000a, b). Subsequent to bend broadening, sediment is bypassed through the channel until the latter is abandoned (Posamentier and Kolla, 2003). Although this model was developed for individual channels, it applies also to channel complexes.

Erosional surfaces flooring channel complexes with a bypass character have been interpreted to represent periods of incision, followed by up to several discrete phases of channel filling (Deptuck et al., 2003, 2007). In situations where high-density (i.e., low mud content) turbidity flows subsequently fill channels, levees are not well developed because mud is not available to construct these features (Posamentier and Kolla, 2003).

Hemipelagites and Muddy Turbidites: Observations

The hemipelagite and muddy turbidite facies is the least variable assemblage and consists of parallel and planar, high- to low-amplitude reflections exhibiting a wedged, lenticular, or tabular external

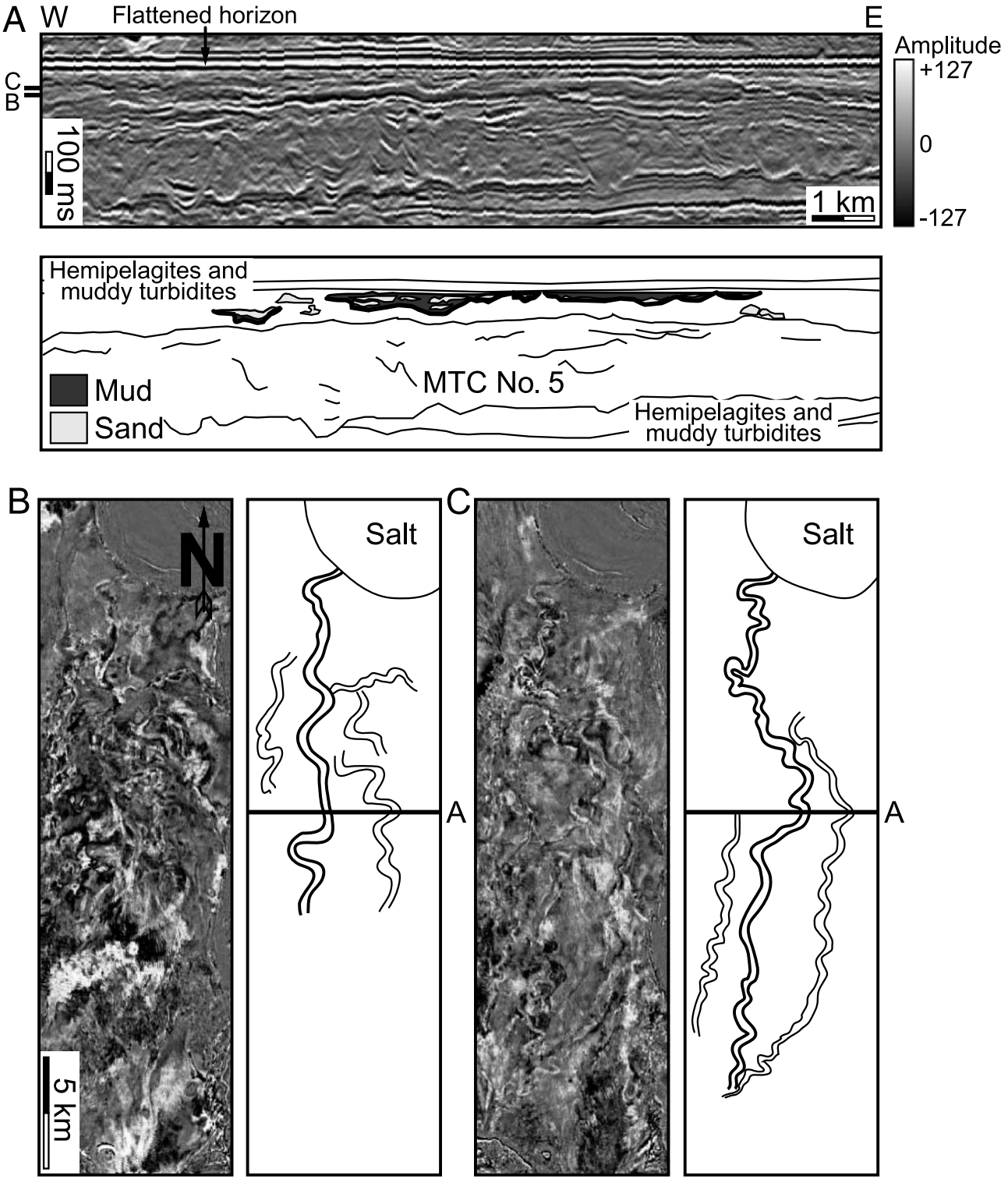

Figure 9. Channelized sandy turbidites showing meandering channels. See Figure 3A for the location of seismic profiles. (A) Flattened profile. Note the location of horizons B and C on the left side of the top panel. (B, C) Horizon slices (plan view) showing individual channels below flattened horizon. Note the increase in sinuosity and length of the main channel up section (from B to C). Scale and north are the same in both panels. MTC = mass transport complex.

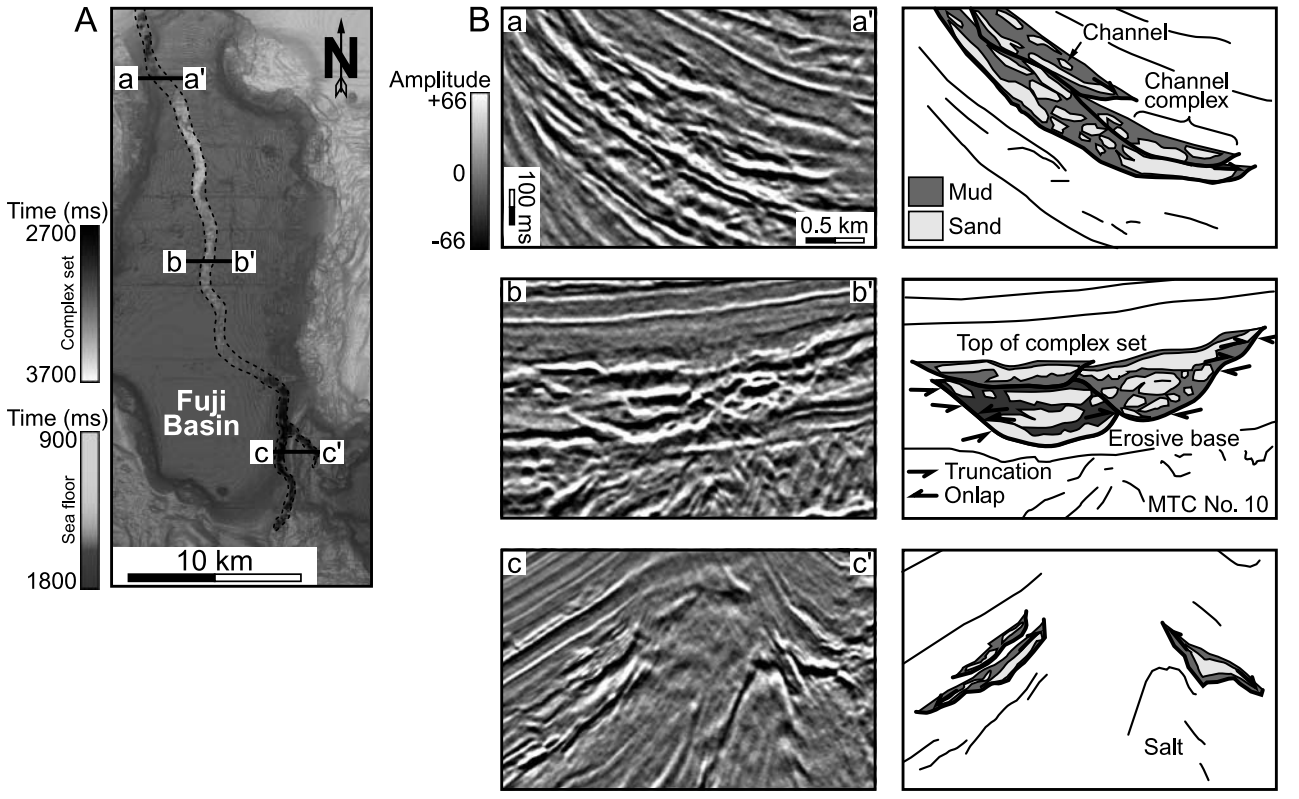

Figure 10. Channelized sandy turbidite facies assemblage showing the set of meandering complexes. (A) Map showing the modern sea floor superimposed over the complex set at depth. (B) Successive uninterpreted and interpreted profiles, showing three channel complexes that constitute the complex set. Toward the north, the complex set is well confined; toward the south, it is weakly confined and separated into discrete complexes. MTC = mass transport complex.

form (see hemipelagites and muddy turbidites in Figure 12). This facies assemblage is characterized by a planar basal surface and high cross-sectional continuity (Table 1).

Successions composing the facies range in thickness from less than 50 ms (~65 m [213 ft]) to more than 500 ms (~665 m [2182 ft]) and in area from a few square kilometers to more than 300 km^2 (116 mi^2). Generally, the assemblage drapes the entire surface area of the basin and thins toward its margins. This facies is nonerosive and exhibits high lateral homogeneity.

Hemipelagites and Muddy Turbidites: Interpretations

This facies is interpreted to represent a combination of mud-rich turbidites, hemipelagic drapes, and condensed intervals (Figure 8). Although the significance of seismically homogeneous facies becomes difficult to determine at depth, our focus here is on the shallow section of the Fuji basin where details are best preserved. Therefore, though high-amplitude continuous reflections could be interpreted as unconfined sand sheets, the lack of channels feeding into these deposits is inconsistent with that interpretation.

AGE CONTROL

Age control within the Fuji basin is provided by two late Pleistocene biostratigraphic datums, one based on the last occurrence of the planktonic coccolith, *Pseudoemiliania lacunosa* (*P. lacunosa*) (~450 ka), and the other on the last occurrence of the benthic foraminifer, *Stilostomella antillea* (*S. antillea*) (~780 ka). These markers, obtained from cuttings while drilling in the southwestern Fuji basin, correlate to two high-amplitude reflections located toward the base of the seismic volume (Figure 12). *Pseudoemiliania lacunosa* is a

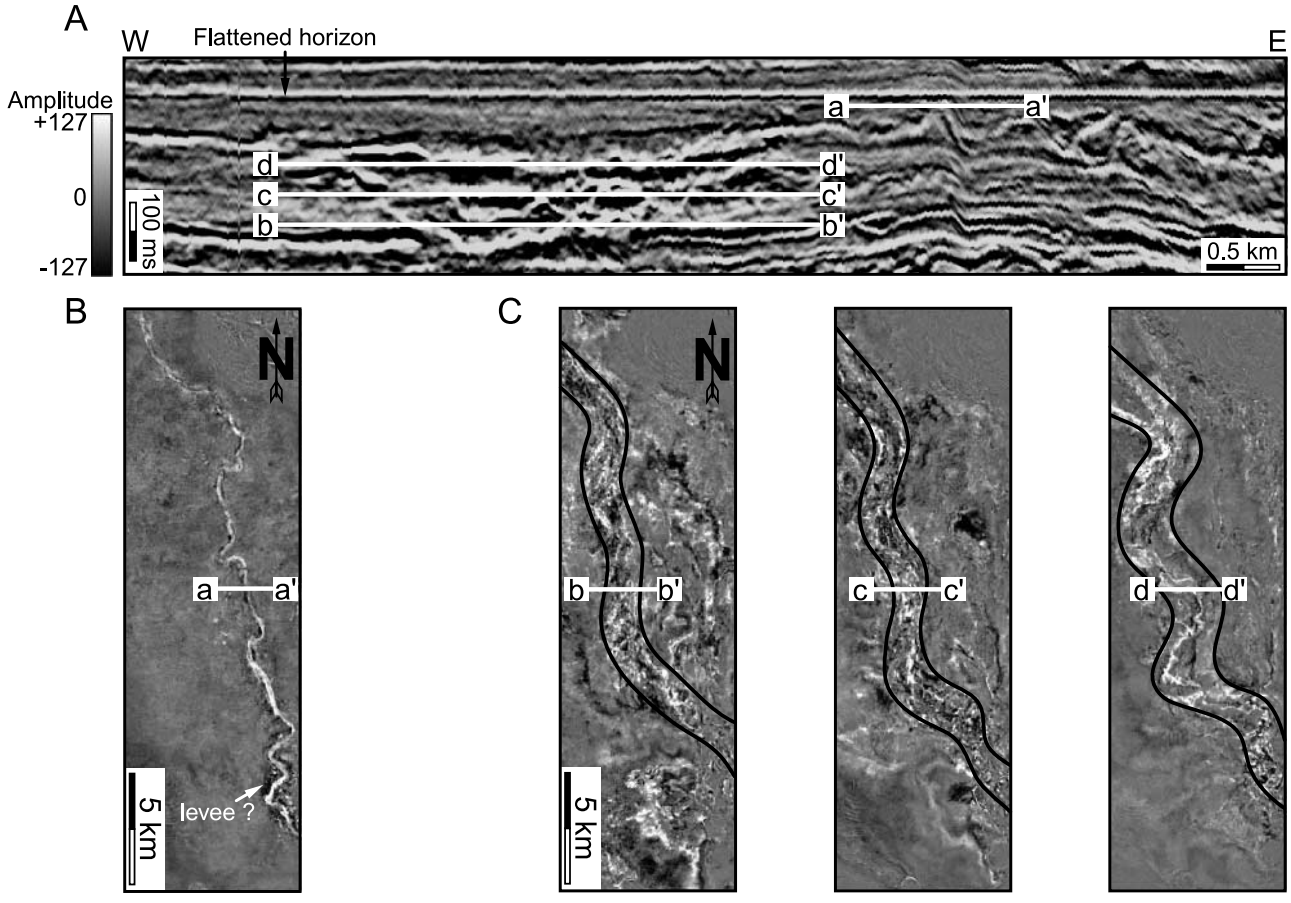

Figure 11. Channelized sandy turbidite facies showing meandering channel and complex set. (A) Flattened profile from Figure 10 (line bb′). (B) Horizon slice (plan view) showing the channel below flattened horizon. (C) Three successive horizon slices (plan view) showing the evolution of the complex set from relatively straight (bb′) to meandering (dd′).

well-documented planktonic coccolith (Thierstein et al., 1977; Scott et al., 1998; Breard et al., 2000) that became globally extinct during marine isotope stage (MIS) 12, approximately 450–470 ka (Thierstein et al., 1977; Beu and Edwards, 1984; Caulet, 1986; Gard, 1988; Black, 1992; Wei et al., 1998; Flores and Marino, 2002; Olson and Smart, 2004). The last occurrence of *P. lacunosa* correlates with the base of MTC no 10. *Stilostomella antillea* is a benthic foraminifer (Hayward, 2002; Witrock et al., 2003; Govindan, 2004; Gavriloff, 2006), with a last occurrence dated as 780 ka during the MIS 16 global extinction (Witrock et al., 2003) of deep-sea benthic foraminifers (Gavriloff, 2006). The *S. antillea* datum correlates with seismic surface no. 45 (S-45).

The largest source of uncertainty within the Fuji basin consists of tying biostratigraphic datums, obtained from cuttings, to seismic sections, for which two-way traveltime is the vertical scale. Available data permit the *P. lacunosa* datum to be as much as 80 ms (~60 m [197 ft]) below its currently interpreted position (T. Elliott, 2008, personal communication). The *S. antillea* datum may be as much as 25 ms (~19 m [62 ft]) above and 80 ms (~60 m [197 ft]) lower than indicated.

SEDIMENT TRANSPORT DIRECTIONS

Based on geometric evidence, MTCs within the Fuji basin are interpreted to have flowed radially into the depocenter. Directions were inferred using large-scale basal incision, small-scale scours, head scarps, fold orientation, and stratigraphic thinning. Basal incision and scours underlying MTCs narrow and terminate down system, implying sediment

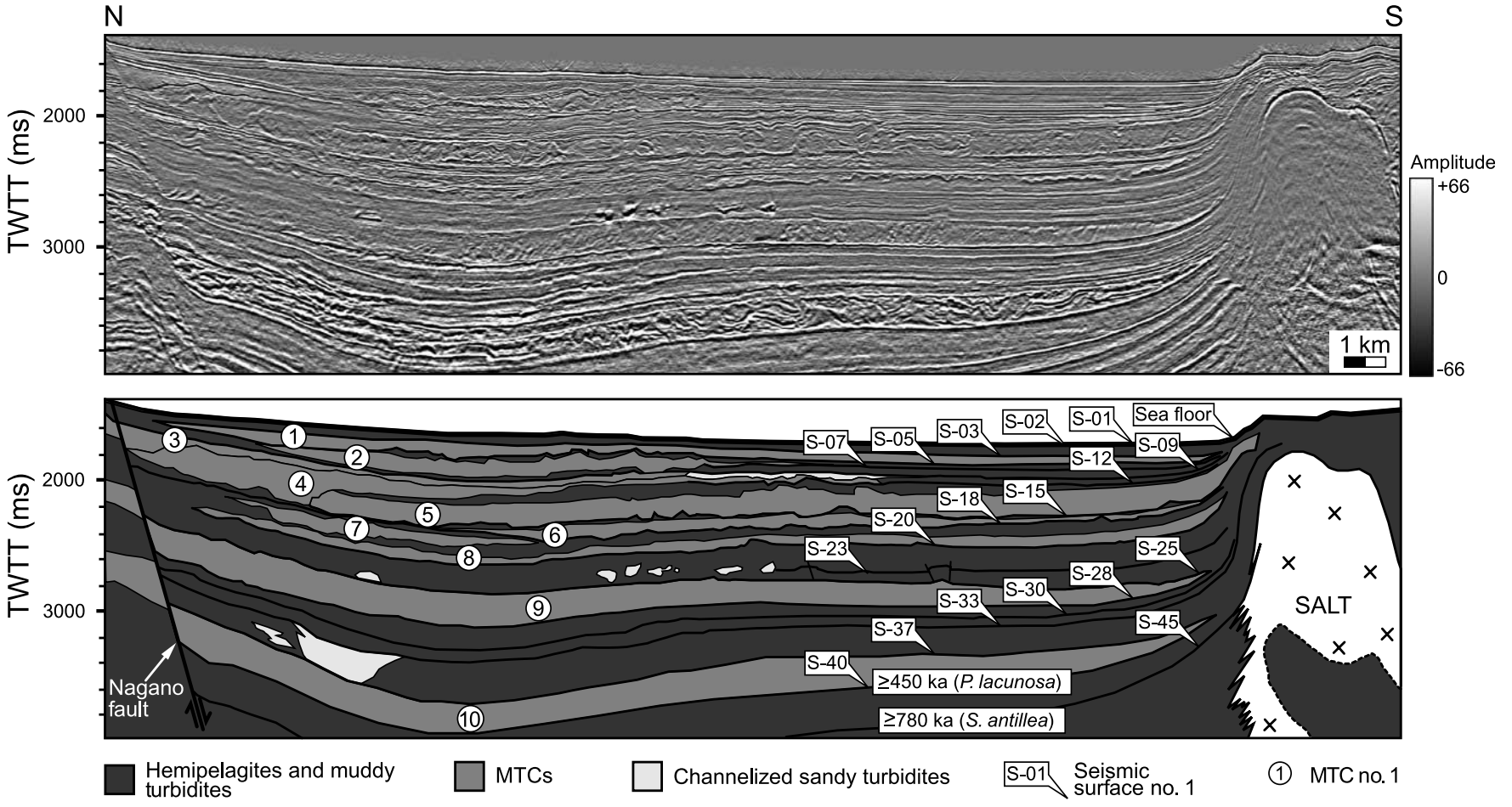

Figure 12. Dip section through the Fuji basin, showing uninterpreted and interpreted seismic profiles. The interpreted section shows the Fuji basin composed primarily of hemipelagites, muddy turbidites, and mass transport complexes (MTCs). Note the presence of *Pseudoemiliania lacunosa* (*P. lacunosa*) and *Stilostomella antillea (S. antillea*) toward the bottom of the section. TWTT = two-way traveltime.

Table 2. Measured Trends of Directional Indicators from Figure 5 and Inferred Sediment Transport Directions for MTC Nos. 9, 8, 5, and 1*

MTC No. 9		MTC No. 8			MTC No. 5		MTC No. 1
Axial Surfaces		Scour Marks (No. 8.1)	Head Scarp	Axial Surface (No. 8.2)	Scour Marks (No. 5.1)	Scour Marks (No. 5.2)	Axial Surfaces
026	048	282	009	037	001	023	008
026	049	293		038	001	024	016
031	049	295		040	002	037	017
033	049	295		041	002	062	018
035	050	298		041	003	062	018
038	050	299		042	005	087	018
040	051	299		042	005	095	020
041	051	302		044	005		022
042	052	304		045	007		022
044	053	305		045	010		
044	056	308		045			
045	057	311		047			
045	059	312		049			
046	061	313		049			
046	064	315		050			
046	068	318					
047	071	320					
047	076	325					
047	116	328					
047	118	330					
047	128						
048	142						
	155						
Mean: 055		Mean: 308		Mean: 044	Mean: 004	Mean: 056	Mean: 018
Inferred transport direction: 180		Inferred transport direction: 308		Inferred transport direction: 314	Inferred transport direction: 004	Inferred transport direction: 056	Inferred transport direction: 288

*The mean was calculated for fold axial surfaces and scours. Transport directions were assumed to be orthogonal to the axial surfaces within MTCs no. 1 and no. 8 and parallel to the scour marks beneath MTCs no. 5 and no. 8. For MTC no. 9, axial surfaces are interpreted to be 135° from the transport direction as a result of deflection around an antecedent structural high. Azimuthal statistics were calculated according to the method of Jones (2006).

transport directions parallel to their longitudinal axes (Posamentier and Kolla, 2003; Moscardelli et al., 2006). Head scarps and folds form roughly orthogonal to transport (Martinez et al., 2005; Moscardelli et al., 2006), although fold orientations are subject to rotation during emplacement and as a result of flow over antecedent topography or a change in gradient. Sediment transport directions are determined with least confidence on the basis of stratigraphic thinning because MTCs thin on both lateral and downdip margins. Directional data for indicators illustrated in Figure 5 are summarized in Table 2 and plotted as rose diagrams in Figure 13.

MTC No. 10

Mass transport complex no. 10, the oldest (Figures 7, 12, 13), is an extrabasinal MTC, with large areal extent. Axial surfaces within the deposit are oriented

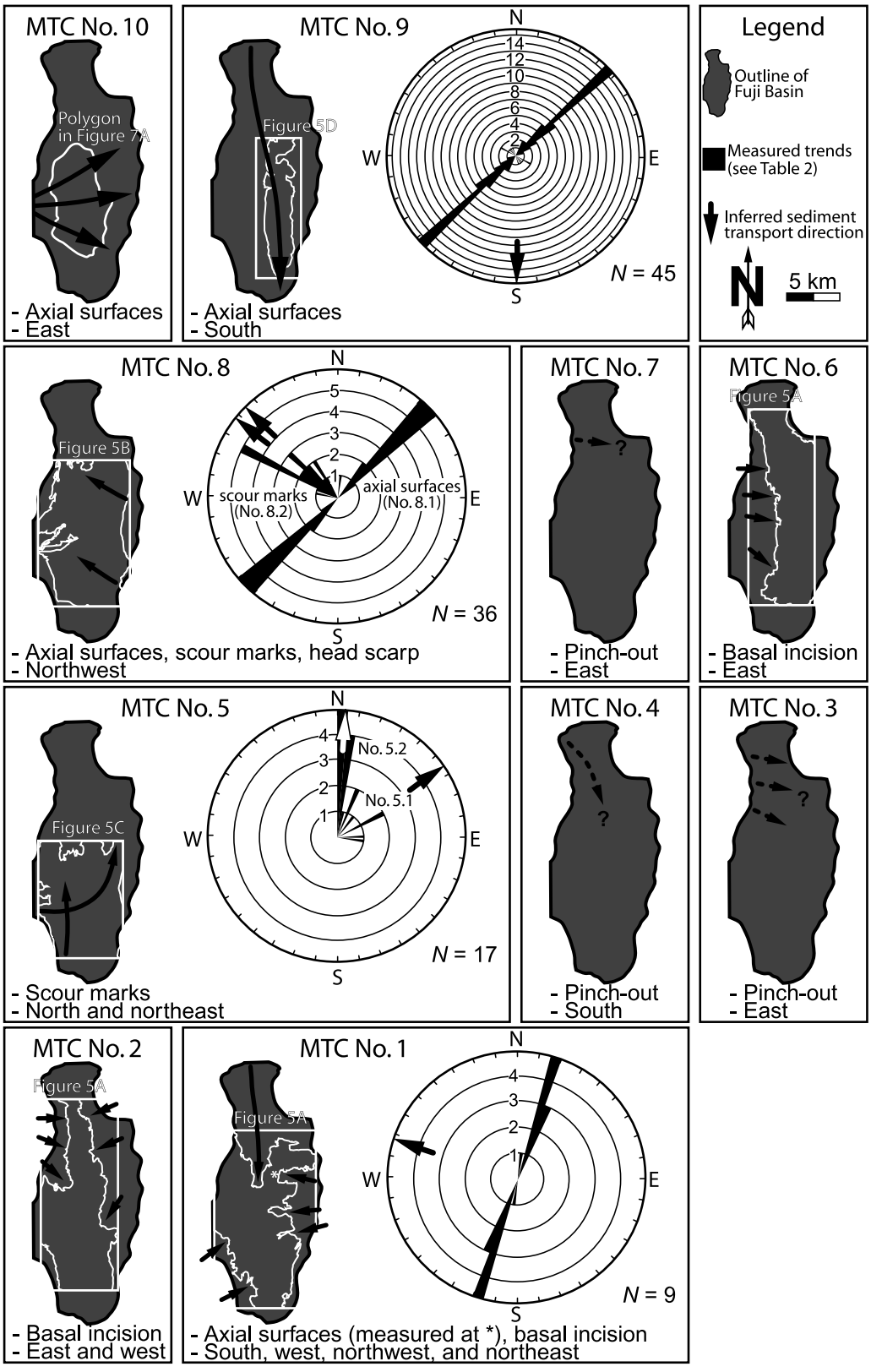

Figure 13. Interpreted sediment transport directions for 10 observed mass transport complexes (MTCs) in the Fuji basin. Features used for inferred sediment transport and propagation directions are given under the outline of the Fuji basin for each MTC. Transport directions for MTCs no. 9, no. 8, no. 5, and no. 1 are based on directional indicators in Figure 5. See Table 2 for tabulated data. Figure 12 shows stratigraphic locations of MTCs.

radially away from the basin's western margin (Figure 7A). Based on the geometry of these features, the MTC is interpreted to have flowed eastward (Figure 13).

MTC No. 9

Mass transport complex no. 9 (Figures 5D, 6, 12, 13) is an extrabasinal MTC, which covers the entire surface area of the Fuji basin. Folds located within the deposit are oriented northeast–southwest (Figures 5D, 6A; rose diagram in Figure 13). Although transport is arguably toward the southeast, orthogonal to fold trend, we infer that their oblique orientation is caused by rotation during emplacement. The MTC is bounded on its eastern margin by a salt-controlled structural high (Figure 6A). As the leading edge of the flowing sediment encountered this topography, folds are thought to have propagated up dip and to have been deflected counterclockwise. A topographic trench on the ridge's western margin (Figure 6A) represents a surficial rift associated with the same solid body rotation. The western side of the MTC is otherwise undeformed.

MTC No. 8

Mass transport complex no. 8 (Figures 5B, 12, 13) is among the thinnest intrabasinal MTCs within the study area. The MTC no. 8 is composed of two laterally amalgamated MTCs: the eastern part of the deposit (no. 8.2) is floored by numerous scours (Figure 5B), whereas the western part (no. 8.1) is associated with folds and a head scarp that serves as a boundary. The MTC no. 8.2 is underlain by several short scours, oriented west–northwest, and abruptly terminating in that direction (Figure 5B; rose diagram in Figure 13). The deposit is bounded on its southeastern margin by a salt-controlled structural high, its inferred local source. The MTC no. 8.1 is floored by structural elements trending northeast–southwest (Figure 5B; rose diagram in Figure 13). The orientations of fold axial surfaces and the dip of the head scarp provide evidence for flow to the west–northwest and for the truncation of MTC no. 8.2, which is inferred to be older on this basis. These interpretations are consistent with the inferred paleoslope.

MTC No. 7

Mass transport complex no. 7 (Figures 12, 13) exists only in the northwestern part of the Fuji basin and is the least laterally persistent intrabasinal MTC recognized. The deposit is delineated on the basis of its wedge-shaped chaotic seismic character and stratigraphic thinning to the east (Figure 13). The MTC no. 7 is inferred to have flowed eastward from the salt-controlled structural high on its western margin.

MTC No. 6

Mass transport complex no. 6 (Figures 5A, 12, 13) is a relatively thin intrabasinal MTC of large areal extent. The deposit shows large-scale basal incision, with relief decreasing to the east on its western margin. Based on basal incision beneath its core and on the proximity of truncation to the northwest and southwest basin flanks, the deposit is interpreted to have been shed eastward in a series of discrete events.

MTC No. 5

Mass transport complex no. 5 (Figures 5C, 12, 13) is the thickest intrabasinal MTC within the Fuji basin. The MTC no. 5 is composed of two laterally amalgamated parts: the lower (no. 5.2) is underlain by linear scours, oriented north and abruptly terminating in that direction; the upper part of the complex (no. 5.1) is floored by curvilinear scours trending east to northeast (Figure 5C; rose diagram in Figure 13). The MTC no. 5.2 is bounded on its southern margin by a salt-controlled structural high (Figure 5C) and is thought to have flowed northward on this basis. The MTC no. 5.1, which exhibits a more complicated evolution, is interpreted to have flowed eastward and to have been deflected by the northern edge of MTC no. 5.2 or by the west-dipping eastern margin of the Fuji basin. In either scenario, no. 5.1 is interpreted to have been derived from the basin's southwestern margin.

MTCS No. 4 and No. 3

Mass transport complexes no. 4 and no. 3 (Figures 12, 13) are wedge-shaped, superimposed intrabasinal complexes that thin abruptly to the southeast. In the northwestern part of the Fuji basin, the deposits appear to be a single MTC. However, their distal, southeastern boundaries are discrete, and they are inferred on this basis to have been sourced locally from the unstable salt-controlled northern and northwestern margins of the basin, respectively (Figure 13).

MTC No. 2

Mass transport complex no. 2 (Figures 5A, 12, 13) is a relatively thin, intrabasinal MTC that thins abruptly to the south. The deposit is associated with prominent large-scale basal incision on its northwestern and eastern margins, shallowing toward the Fuji basin's depocenter. This geometry implies numerous radial sediment sources.

MTC No. 1

Mass transport complex no. 1, the youngest of the 10 examples (Figures 5A, 12, 13), is a thin, intrabasinal complex of large areal extent. Prominent large-scale basal incisions are present on its northern, eastern, and southwestern margins, with erosional relief decreasing radially toward the Fuji basin's center. North-trending folds are locally truncated at the distal edge of the deposit (Figure 5A). The MTC no. 1 is interpreted as a radially sourced and laterally amalgamated composite of several events.

DISCUSSION

Passive salt motion accounts better for the volumetric abundance of MTCs compared with other facies in the Fuji basin, for their varied directions of emplacement, for their frequency during the last four 100-k.y. cycles of sea level change, and for the manner in which the basin evolved than currently popular eustatic and steady-state bathymetric models.

Halokinetic Autocyclicity

Halokinetic autocyclicity is identified as the primary control on stratigraphic architecture in the Fuji basin. According to this hypothesis, slope stability and patterns of sediment accumulation are governed locally by the 3-D motion of the salt (Figure 14). At the beginning of each cycle, the accumulation of hemipelagites and muddy turbidites unevenly loads preexisting bathymetry. Subsidence in the depocenter displaces the salt at depth and induces passive uplift and oversteepening of basin margins. Margin failure results in intrabasinal MTCs, which flow radially toward and pond within the depocenter. Loading and compaction together result in additional subsidence. The cycle repeats with renewed accumulation of fine-grained sediments. At least eight such cycles have been documented in the Fuji basin since 450 ka (MTCs no. 8 to 1).

Giles and Lawton (2002) reported similar salt-driven deposition adjacent to the El Papalote diapir in northeastern Mexico. Halokinetics were a fundamental factor in that example in controlling the distribution of upper Cretaceous to Paleogene MTCs, but differences exist relative to the Fuji basin. For example, the La Popa Basin contains shallow-water siliciclastic deposits punctuated by volumetrically smaller carbonate MTCs shed from the El Papalote diapir. Diapiric material may have been extruded onto the sea floor and motion of the salt enhanced by middle to late Maastrichtian tectonic shortening.

Salt motion is also a factor at a scale larger than the Fuji basin through differential loading more generally of sediments beneath the outer shelf and upper slope (Tripsanas et al., 2004) and through the concomitant triggering of sediment failure events. Although the distinction between intra- and extrabasinal MTCs is somewhat arbitrary, and in practical terms, a function of the dimensions of the 3-D seismic volume being studied, extrabasinal MTCs such as no. 10 and 9 in this study appear to relate to salt motion at a regional scale instead of proximity to a particular salt structure. The tendency for the most recent MTCs to be intrabasinal instead of extrabasinal may relate to the exhaustion of the salt source beneath the Fuji basin by 0.2 Ma (McBride, 1997).

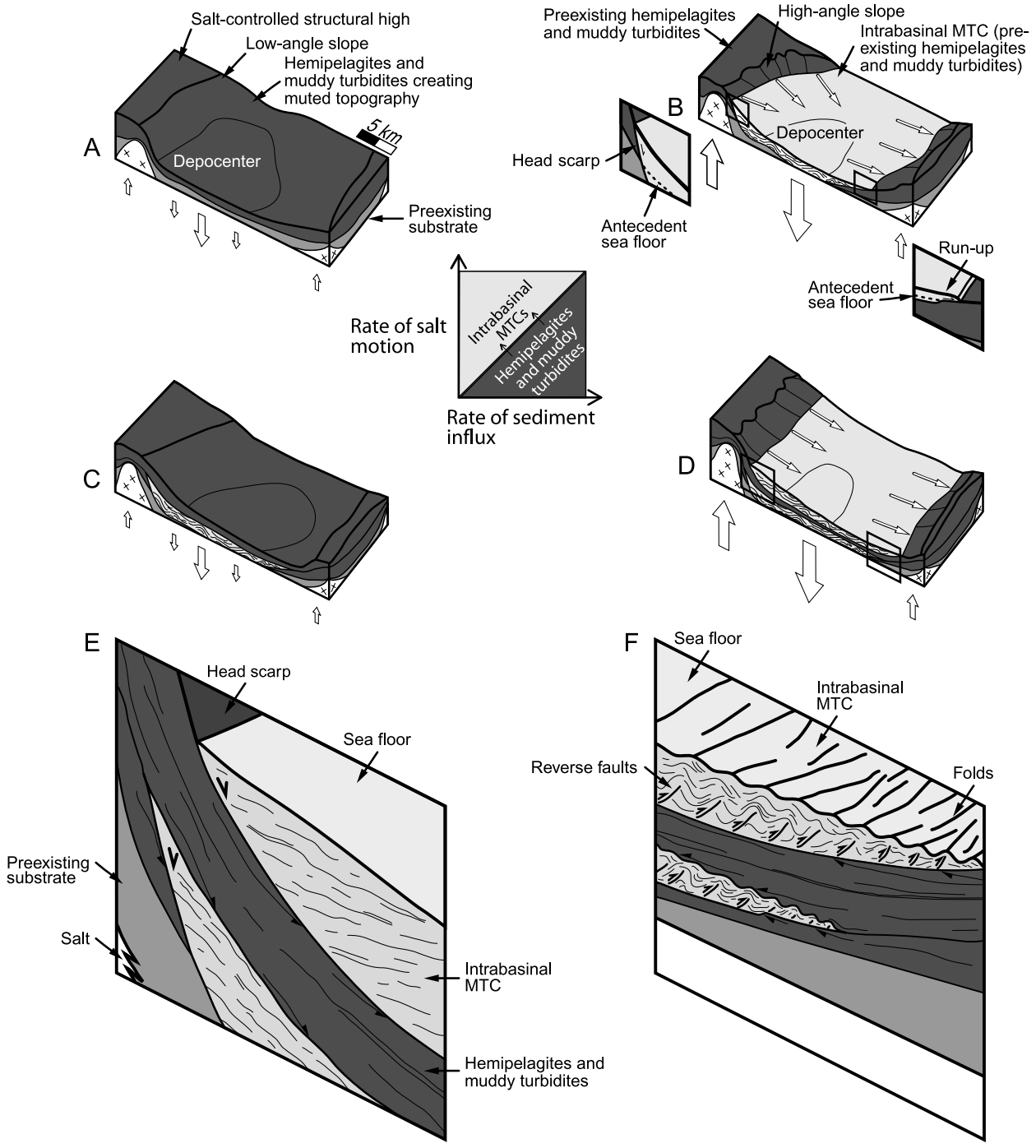

Figure 14. Conceptual model showing salt-controlled cyclic generation of intrabasinal mass transport complexes (MTCs). (A) Hemipelagites and muddy turbidites drape the underlying substrate, creating muted topography. Loading creates subsidence (down arrows) in the depocenter and associated passive salt uplift at the basin margins (up arrows). (B) Basin margins oversteepen, leading to the subsequent failure of the left flank. Failure on the margin creates an intrabasinal MTC, which propagates toward the depocenter; preferential ponding of the MTC creates depocenter migration and narrowing. Subsequent to MTC deposition, loading creates increased subsidence and associated compaction in the depocenter and uplift at basin margins. Uplift at basin margins creates differential compaction above salt, accounting for stratigraphic thinning. (C) Hemipelagites and muddy turbidites drape the underlying topography, muting preexisting substrate (i.e., MTC). (D) Generation of a second intrabasinal MTC caused by basin margin oversteepening and subsequent failure. (E) Magnification of the box at the left of panel D, showing resultant stratigraphy of the trailing edge of the MTC. (F) Magnification of the box at the right side of panel D, showing resultant stratigraphy of the leading edge of the MTC. Note the truncation at the base of the MTC and onlap onto the top of the deposit.

Eustasy

Sequence stratigraphic models for deep-water depositional systems use facies assemblages as proxies for the interpretation of eustatic cycles and shoreline position (Weimer, 1990; Posamentier and Kolla, 2003). According to this view, at eustatic high stands, the accumulation of coarse-grained sediments is thought to occur preferentially in shallow-marine environments. Deep-water off-shelf settings are relatively starved and characterized for the most part by slowly accumulating hemipelagic sediments. Falling sea level leads to progradation and shoaling and, in slope settings, to the development of overpressure as pore fluids in low-permeability mud fail to remain in equilibrium with the decreasing externally imposed pressure. This leads in turn to upper slope failure and to the development of MTCs (Weimer, 1990; Posamentier and Kolla, 2003). At eustatic low stands, shorelines are thought to extend close to the shelf-slope break. Coarse-grained sediment bypasses the shelf via incised valleys and is delivered to the slope via turbidity currents. Posamentier and Kolla (2003) hypothesized that following turbidite deposition, rapid rises of sea level may produce "disequilibrium conditions" on the upper slope through water and sediment loading, leading to a second generation of MTCs. The mechanism by which MTCs are generated during this interval remains unclear however. Hemipelagic sedimentation resumes during eustatic high stands.

These ideas lead to testable corollaries. A vertical succession through a deep-water sequence should include the following elements in ascending order: a condensed section, an MTC, a turbidite complex, and in some cases, a second MTC and condensed section. Sequence boundaries underlying MTCs are interpreted as laterally persistent, well beyond the dimensions of any particular complex, and of temporal significance. The pattern repeats because eustatic change is the principal modulator of sedimentation at continental margins (Posamentier and Kolla, 2003). In the absence of sand, deep-water systems may lack turbidites and consist primarily of debris flows (Posamentier and Kolla, 2003).

The main difficulty with the eustatic model is that it fails to account for the volumetric abundance of MTCs in the Fuji basin, for their varied directions of emplacement, or for their frequency. Since the late Pleistocene (~450 ka), there have been four major eustatic cycles (Figure 15A), with a prominent eccentricity-dominated (100 k.y.) signature (Miller et al., 2005). Assuming that sediment was available throughout each eustatic cycle and that the resultant stratigraphy was preserved, one would expect to see between four and eight MTCs sourced regionally from the upper slope flowing southward down the regional paleoslope (Figure 16). Yet, 10 MTCs are present in the Fuji basin in the late Pleistocene to Holocene interval, and they were sourced for the most part from the flanks of the basin (Figure 13).

Studies of late Pleistocene deposits southeast of the ancestral Mississippi River, offshore Louisiana, lead to similar conclusions. Using log, core, and biostratigraphic data, Scott et al. (1998) found that the timing of erosional surfaces (i.e., sequence boundaries) is aperiodic and not associated with any single Milankovitch frequency. These authors concluded that a suite of sedimentary processes, and not simply continental glacial cycles, is responsible for the stratigraphic evolution of passive continental margins.

Bathymetry

An alternative to the eustatic model is the idea that sedimentation in a minibasin is controlled by its steady-state longitudinal (dip) bathymetric profile (Winker and Booth, 2000; Mallarino et al., 2006) through a three-part evolution from ponded basin fill to perched slope fill to complete bypass (Beaubouef and Friedmann, 2000). According to this view, coarse-grained and slumped sediment initially becomes ponded below the basin's spill point (Figure 15B, top). Hemipelagic sediment, in contrast, is able to accumulate both above and below this depth. Once the minibasin is filled, sediment perches from above the spill point to the local slope profile of the basin (Figure 15B, middle). As the minibasin enters a phase of bypass, preexisting deposits are eroded basinward of the regional (equilibrium) profile and transported downslope (Figure 15B, bottom).

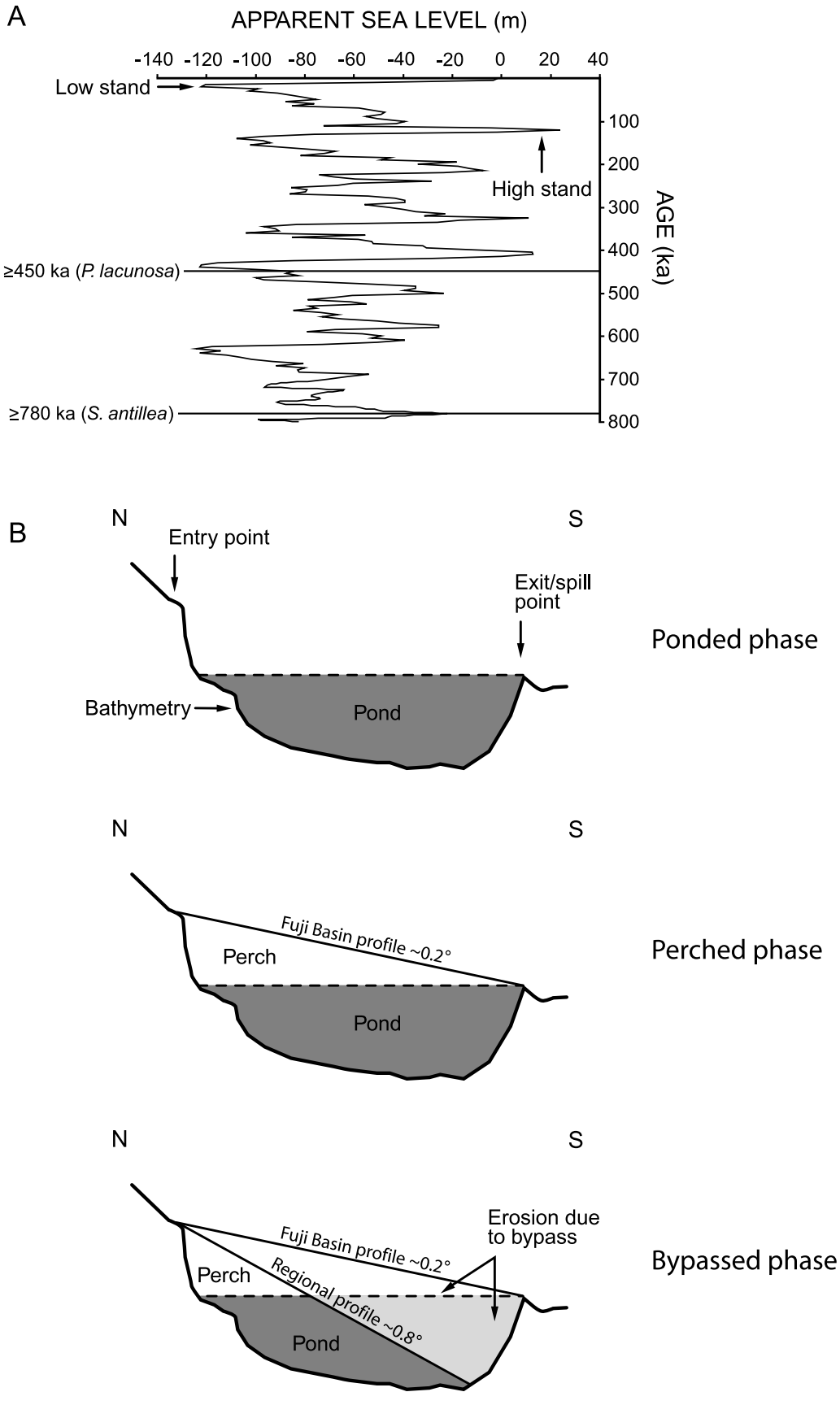

Figure 15. Quaternary sea-level fluctuations and steady state bathymetric profile for Fuji basin. (A) Apparent sea level curve (eustasy plus water loading) showing eccentricity-dominated signature, 100-k.y. cycles (Miller et al., 2005). Timing uncertainties in sea level curve are approximately ±5 k.y., whereas amplitude errors range from ±10% (low stands) to +20% (high stands) (K. G. Miller, 2007, personal communication). (B) Evolution of the Fuji basin, showing ponded basin fill (top) to perched slope fill (middle) to complete bypass (bottom), following Beaubouef and Friedmann (2000). Note that the Fuji basin profile is taken from present-day bathymetry, whereas the dip of the regional profile was taken from Prather et al. (1998). *P. lacunosa* = *Pseudoemiliania lacunosa*; *S. antillea* = *Stilostomella antillea*.

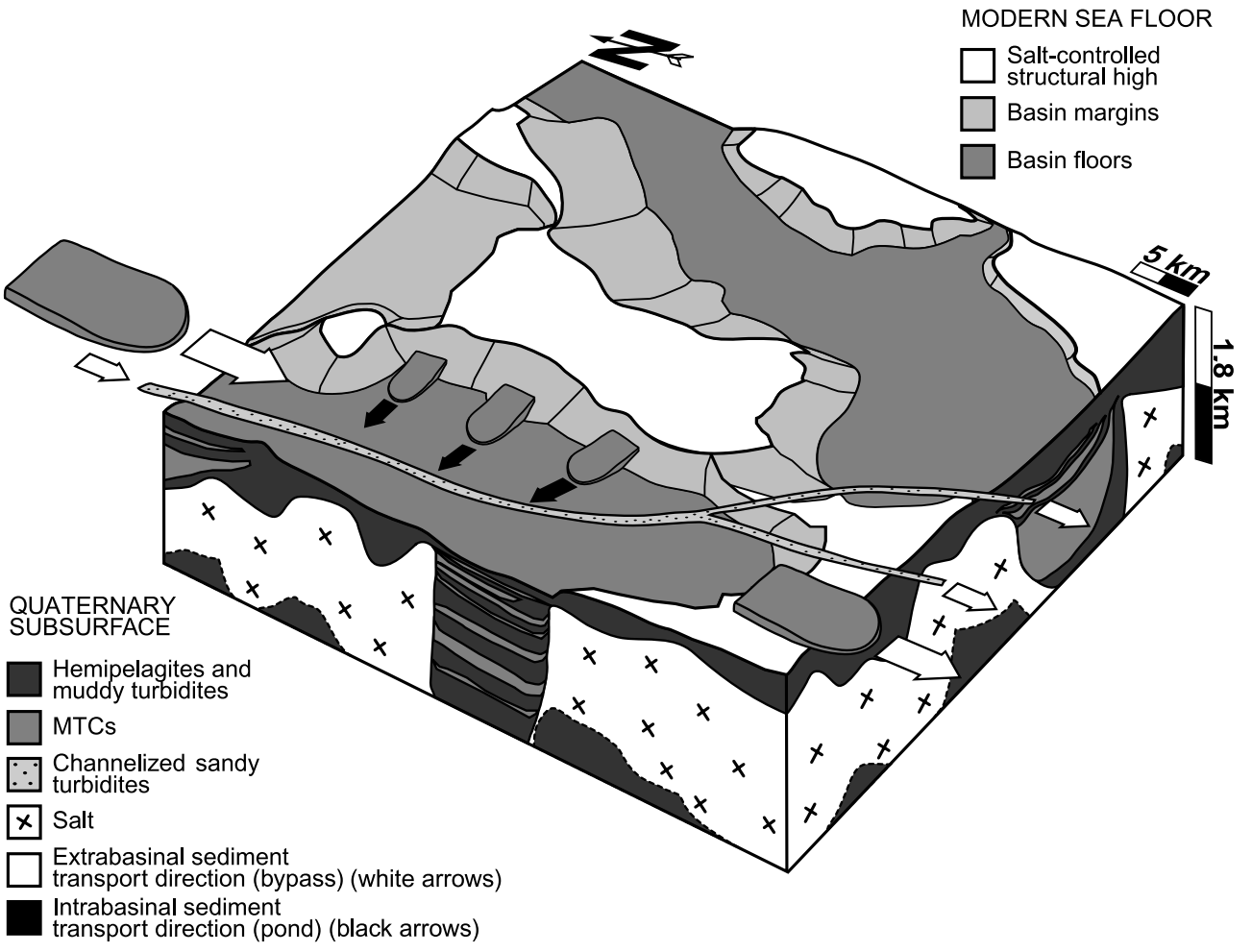

Figure 16. Conventional view of sediment transport directions for extrabasinal mass transport complexes (MTCs), intrabasinal MTCs, and channelized sandy turbidites. This model assumes that MTCs both bypass and pond in the Fuji basin, whereas channelized sandy turbidites primarily bypass to the south. Compare with Figure 14, which shows that most MTCs are derived from basin margins as a result of passive salt motion.

Fundamental assumptions of the bathymetric model are that the gradient of intraslope basins does not vary significantly along strike or at any given location at time scales of up to 250–750 k.y. (Winker and Booth, 2000), and that deposition outpaces subsidence. Our work in the Fuji basin suggests that these assumptions are unrealistic. The depocenter and margins of intraslope basins have different depositional histories that cannot be understood using a single (or simple) two-dimensional profile. Depocenters are sites of net deposition and an archive of basin-margin instability (e.g., intrabasinal MTCs). Basin flanks range from depositional to erosional, depending on patterns of salt motion at depth. This sediment-controlled motion enabled the Fuji basin to subside and subsequently pond sediments for the last approximately 780 k.y. In each case, the controls on sedimentation are inherently variable with respect to time.

Application of the bathymetric model to the Fuji basin presents a problem also because it cannot explain the spatial and temporal evolution of the basin. Using the bathymetric concept implies that the Fuji basin should have low preservation potential as a result of excessive bypass (Figure 15B, bottom). Yet, the only deposits that have bypassed the Fuji basin during the last approximately 780 k.y. are those associated with the channelized sandy turbidite complex, with flow to the south and southeast

(Figures 10a, 16). Other deposits within the basin (i.e., intrabasinal MTCs) were ponded as a result of high subsidence rates. Therefore, the temporal evolution of the basin must be understood in terms of dynamic loading-driven basin-margin uplift and subsequent failure and not through the use of a steady-state bathymetric profile.

RESERVOIR ANALOGS, SEALS, AND DRILLING HAZARDS

The principal reservoir analogs in the late Pleistocene of the Fuji basin are the volumetrically minor (5%) channelized sandy turbidites. The remaining facies (hemipelagites, muddy turbidites, and MTCs) are expected to be of low porosity and permeability and to act as seals both below and above reservoir sands at stratigraphic pinch-outs (e.g., the prominent channelized sandy turbidite overlying MTC no. 10, left side of Figure 12). To the extent that stratigraphic architecture is locally controlled, as we argue is the case in this article, the hydrocarbon prospectivity of salt-controlled minibasins is expected to be highly variable.

Overpressured MTCs constitute potential drilling hazards. Such hazards are hard to avoid when MTCs account for 45% of the total volume of deposits. However, risks can be mitigated by drilling through the margins of depocenters and preferentially through intrabasinal MTCs, which appear to be more cohesive than deposits characterized by longer run-out distances (Gee et al., 1999; Pirmez et al., 2004).

CONCLUSIONS

The Fuji basin, an upper Pliocene to Holocene salt-withdrawal intraslope minibasin in north-central Green Canyon, Gulf of Mexico, collected more than 1.8 km (~5900 ft) of sediment during the last approximately 780 k.y. The basin fill consists of approximately of 45% MTCs, 5% channelized sandy turbidites, and 50% hemipelagites and muddy turbidites. The MTCs are interpreted to be halokinetically triggered, flowing radially toward the depocenter, either from the basin flanks (i.e., intrabasinal) or as a result of larger-scale salt motion (i.e., extrabasinal). Sandy turbidites are channelized at a considerable range of scales. An amalgamated set of three sandy turbidite channel complexes located toward the bottom of the volume represents the major sand delivery to the basin. Hemipelagites and muddy turbidites are of relatively uniform thickness at basin scale and constitute the most homogeneous seismic facies in the Fuji basin.

Passive salt motion, as opposed to eustasy and steady-state bathymetry, is inferred to be the primary control on the stratigraphic architecture in the Fuji basin. Eustatic models fail primarily when considering the number of MTCs deposited since the late Pleistocene and the directions of emplacement of these deposits. Bathymetric models fall short because they use static two-dimensional longitudinal (dip) profiles to understand the dynamic and 3-D evolution of minibasins.

REFERENCES CITED

Acosta, Z., 1994, Sequence stratigraphy of the Plio-Pleistocene sediments in north central Green Canyon and western Ewing Bank, northern Gulf of Mexico: Masters thesis, University of Colorado, Boulder, Colorado, 187 p.

Beaubouef, R. T., and S. J. Friedmann, 2000, High resolution seismic/sequence stratigraphic framework for the evolution of Pleistocene intra slope basins, western Gulf of Mexico: Depositional models and reservoir analogs, *in* P. Weimer, R. M. Slatt, J. Coleman, N. C. Rosen, H. Nelson, A. H. Bouma, M. J. Styzen, and D. T. Lawrence, eds., Deep-water reservoirs of the world: Proceedings of the 20th Annual Research Conference, Gulf Coast Section Society for Sedimentary Geology Foundation, p. 40–60.

Beu, A. G., and A. R. Edwards, 1984, New Zealand Pleistocene and late Pliocene glacio-eustatic cycles: Palaeogeography, Palaeoclimatology, Palaeoecology, v. 46, p. 119–142, doi:10.1016/0031-0182(84)90030-0.

Bevc, D., M. M. Fliedner, A. M. Popovici, and B. Biondi, 2003, Optimal velocity models for wavefield continuation migration: European Association of Geoscientists and Engineers/Society of Exploration Geophysicists Research Workshop, Trieste, Italy, August 31–September 4, 2003, p. 1–4.

Bird, D. E., K. Burke, S. A. Hall, and J. F. Casey, 2005, Gulf of Mexico tectonic history: Hotspot tracks, crustal boundaries, and early salt distribution: AAPG Bulletin, v. 89, p. 311–328, doi:10.1306/10280404026.

Black, T. M., 1992, Chronology of the middle Pleistocene

Kidnappers Group, New Zealand and correlation to global oxygen isotope stratigraphy: Earth and Planetary Science Letters, v. 109, p. 573–584, doi:10.1016/0012-821X(92)90115-C.

Breard, S. Q., A. D. Callender, R. A. Denne, and M. J. Nault, 2000, Gulf of Mexico Basin late Tertiary deep-water biostratigraphic zonation: Relationship to standard shelf foraminiferal and calcareous nannofossil marker terminology, *in* P. Weimer, R. M. Slatt, J. Coleman, N. C. Rosen, H. Nelson, A. H. Bouma, M. J. Styzen, and D. T. Lawrence, eds., Deep-water reservoirs of the world: Proceedings of the 20th Annual Research Conference, Gulf Coast Section Society for Sedimentary Geology Foundation, p. 116–126.

Buffler, R. T., and D. S. Sawyer, 1985, Distribution of crust and early history, Gulf of Mexico: Gulf Coast Association of Geological Societies Transactions, v. 35, p. 333–344.

Bünz, S., J. Mienert, P. Bryn, and K. Berg, 2005, Fluid flow impact on slope failure from 3D seismic data: A case study in the Storegga Slide: Basin Research, v. 17, p. 109–122, doi:10.1111/j.1365-2117.2005.00256.x.

Carbotte, S. M., et al., 2004, New integrated data management system for Ridge2000 and MARGINS research: EOS, v. 85, no. 51, p. 553, 559, doi:10.1029/2004EO510002.

Caulet, J. P., 1986, A refined radiolarian biostratigraphy for the Pleistocene of the temperate Indian Ocean: Marine Micropaleontology, v. 11, p. 217–229, doi:10.1016/0377-8398(86)90016-2.

Deptuck, M. E., G. S. Steffens, M. Barton, and C. Pirmez, 2003, Architecture and evolution of upper fan channel-belts on the Niger Delta slope and in the Arabian Sea: Marine and Petroleum Geology, v. 20, p. 649–676, doi:10.1016/j.marpetgeo.2003.01.004.

Deptuck, M. E., Z. Sylvester, C. Pirmez, and C. O'Byrne, 2007, Migration-aggradation history and 3-D seismic geomorphology of submarine channels in the Pleistocene Benin-major Canyon, western Niger Delta slope: Marine and Petroleum Geology, v. 24, p. 406–433, doi:10.1016/j.marpetgeo.2007.01.005.

Diegel, F. A., J. F. Karlo, D. C. Schuster, R. C. Shoup, and P. R. Tauvers, 1995, Cenozoic structural evolution and tectono-stratigraphic framework of the northern Gulf Coast continental margin, *in* M. P. A. Jackson, D. G. Roberts, and S. Snelson, eds., Salt tectonics: A global perspective: AAPG Memoir 65, p. 109–151.

Expedition 308 Scientists, 2005, Overpressure and fluid flow processes in the deep water Gulf of Mexico: Slope stability, seeps, and shallow-water flow: Integrated Ocean Drilling Program Preliminary Report 308, doi: 10:2204/iodp.pr.308.2005.

Feng, J., R. T. Buffler, and M. A. Kominz, 1994, Laramide orogenic influence on late Mesozoic–Cenozoic subsidence history, western deep Gulf of Mexico basin: Geology, v. 22, p. 359–362, doi:10.1130/0091-7613(1994)022<0359:LOIOLM>2.3.CO;2.

Flores, J. A., and M. Marino, 2002, Pleistocene calcareous nannofossil stratigraphy for the ODP leg 177 (Atlantic sector of the Southern Ocean): Marine Micropaleontology, v. 45, p. 191–224, doi:10.1016/S0377-8398(02)00030-0.

Gard, G., 1988, Late Quaternary calcareous nannofossil biozonation, chronology, and paleo-oceanography in areas north of the Faeroe-Iceland Ridge: Quaternary Science Reviews, v. 7, p. 65–78, doi:10.1016/0277-3791(88)90094-7.

Gavriloff, I. J. C., 2006, The mid-Pleistocene "*Stilostomella* extinction event" in the southeast Pacific Ocean: A review: Anuário do Instituto de Geociências, v. 29, p. 490.

Gee, M. J. R., D. G. Masson, A. B. Watts, and P. A. Allen, 1999, The Saharan debris flow: An insight into the mechanics of long runout submarine debris flows: Sedimentology, v. 46, p. 317–335, doi:10.1046/j.1365-3091.1999.00215.x.

Gee, M. J. R., R. L. Gawthorpe, and J. S. Friedmann, 2005, Giant striations at the base of a submarine landslide: Marine Geology, v. 214, p. 287–294, doi:10.1016/j.margeo.2004.09.003.

Giles, K. A., and T. F. Lawton, 2002, Halokinetic sequence stratigraphy adjacent to the El Papalote diapir, northeastern Mexico: AAPG Bulletin, v. 86, p. 823–840.

Govindan, A., 2004, Miocene deep water agglutinated foraminifera from offshore Krishna-Godavari Basin, India: Micropaleontology, v. 50, p. 213–252.

Haflidason, H., H. P. Sejrup, A. Nygård, J. Mienert, P. Bryn, R. Lien, C. F. Forsberg, K. Berg, and D. Masson, 2004, The Storegga Slide: Architecture, geometry and slide development: Marine Geology, v. 213, p. 201–234, doi:10.1016/j.margeo.2004.10.007.

Hayward, B. W., 2002, Late Pliocene to middle Pleistocene extinctions of deep-sea benthic foraminifera ("*Stilostomella* extinction") in the southwest Pacific: Journal of Foraminiferal Research, v. 32, p. 274–307, doi:10.2113/32.3.274.

Jones, T. A., 2006, MATLAB functions to analyze directional (azimuthal) data: I. Single-sample inference: Computers and Geosciences, v. 32, p. 166–175, doi:10.1016/j.cageo.2005.06.009.

Mallarino, G., R. T. Beaubouef, A. W. Droxler, V. Abreu, and L. Labeyrie, 2006, Sea level influence on the nature and timing of a minibasin sedimentary fill (northwestern slope of the Gulf of Mexico): AAPG Bulletin, v. 90, p. 1089–1119, doi:10.1306/02210605058.

Marine Geoscience Data System, 2008, Explore our planet with GeoMapApp: Lamont-Doherty Earth Observatory, Columbia University, New York: http://www.geomapapp.org/index.htm (accessed December 4, 2007).

Martinez, J. F., J. A. Cartwright, and B. Hall, 2005, 3D seismic interpretation of slump complexes, examples from the continental margin of Israel: Basin Research, v. 17, p. 83–108, doi:10.1111/j.1365-2117.2005.00255.x.

McBride, B. C., 1997, The geometry and evolution of allochthonous salt and its impact on petroleum systems, northern Gulf of Mexico basin, studies in three- and four-dimensional analysis: Ph.D. dissertation, University of Colorado, Boulder, Colorado, 275 p.

McDonnell, A., R. G. Loucks, and W. E. Galloway, 2008, Paleocene to Eocene deep-water slope canyons, western Gulf of Mexico: Further insights for the provenance of deep-water offshore Wilcox Group plays: AAPG Bulletin, v. 92, p. 1169–1189, doi:10.1306/05150808014.

McHugh, C. M. G., J. E. Damuth, and G. S. Mountain, 2002,

Cenozoic mass-transport facies and their correlation with relative sea-level change, New Jersey continental margin: Marine Geology, v. 184, p. 295–334, doi:10.1016/S0025-3227(01)00240-7.

Miller, K. G., M. A. Kominz, J. V. Browning, J. D. Wright, G. S. Mountain, M. E. Katz, P. J. Sugarman, B. S. Cramer, N. Christie-Blick, and S. F. Pekar, 2005, The Phanerozoic record of global sea-level change: Science, v. 301, p. 1293–1298, doi:10.1126/science.1116412.

Moscardelli, L., L. Wood, and P. Mann, 2006, Mass-transport complexes and associated processes in the offshore area of Trinidad and Venezuela: AAPG Bulletin, v. 90, p. 1059–1088, doi:10.1306/02210605052.

Nissen, S. E., N. L. Haskell, C. T. Steiner, and K. L. Cortelli, 1999, Debris flow outrunner blocks, glide tracks, and pressure ridges identified on the Nigerian continental slope using 3-D seismic coherency: The Leading Edge, v. 18, no. 5, p. 595–599, doi:10.1190/1.1438343.

Olson, H. C., and C. W. Smart, 2004, Pleistocene climatic history reflected in planktonic Foraminifera from ODP site 1073 (leg 174A), New Jersey margin, NW Atlantic Ocean: Marine Micropaleontology, v. 51, p. 213–238, doi:10.1016/j.marmicro.2003.11.002.

Peakall, J., W. D. McCaffrey, and B. C. Kneller, 2000a, A process model for the evolution, morphology and architecture of sinuous submarine channels: Journal of Sedimentary Research, v. 70, p. 434–448, doi:10.1306/2DC4091C-0E47-11D7-8643000102C1865D.

Peakall, J., W. D. McCaffrey, B. C. Kneller, C. E. Stelting, T. R. McHargue, and W. J. Schweller, 2000b, A process model for the evolution of submarine fan channels: Implications for sedimentary architecture, *in* A. H. Bouma and C. G. Stone, eds., Fine-grained turbidite systems: AAPG Memoir 72, p. 73–87.

Pirmez, C., J. Marr, C. Shipp, and F. Kopp, 2004, Observations and numerical modeling of debris flows in the Na Kika Basin, Gulf of Mexico: Annual Offshore Technology Conference, Houston, Texas, Offshore Geology Foundation (OTC) Paper 16749, p. 1–13.

Posamentier, H. W., and V. Kolla, 2003, Seismic geomorphology and stratigraphy of depositional elements in deep-water settings: Journal of Sedimentary Research, v. 73, p. 367–388, doi:10.1306/111302730367.

Prather, B. E., J. R. Booth, G. S. Steffens, and P. A. Craig, 1998, Classification, lithologic calibration, and stratigraphic succession of seismic facies of intraslope basins, deep-water Gulf of Mexico: AAPG Bulletin, v. 82, p. 701–728.

Salvador, A., 1987, Late Triassic–Jurassic paleogeography and origin of Gulf of Mexico Basin: AAPG Bulletin, v. 71, p. 419–451.

Salvador, A., ed., 1991, The Gulf of Mexico Basin: Boulder, Colorado, Geological Society of America, The Geology of North America, v. J, 568 p.

Scott, R. W., J. M. Combes, and S. E. Nissen, 1998, High-precision chronostratigraphy of a late Pleistocene shelf-edge delta, Louisiana: Journal of Sedimentary Research, v. 68, p. 596–602.

Soto, G., 1997, 3-D seismic stratigraphic interpretation of Pleistocene sediments, Fuji minibasin, central Green Canyon, northern deep Gulf of Mexico: Masters thesis, University of Colorado, Boulder, Colorado, 176 p.

Thierstein, H. R., K. Geitzenauer, B. Molfino, and N. J. Shackleton, 1977, Global synchroneity of late Quaternary coccolith datum levels: Validation by oxygen isotopes: Geology, v. 5, p. 400–404, doi:10.1130/0091-7613(1977)5<400:GSOLQC>2.0.CO;2.

Tripsanas, E. K., W. R. Bryant, and B. A. Phaneuf, 2004, Slope-instability processes caused by salt movements in a complex deep-water environment, Bryant Canyon area, northwest Gulf of Mexico: AAPG Bulletin, v. 88, p. 801–823, doi:10.1306/01260403106.

Wei, K. Y., T. Q. Lee, and the shipboard scientific party of IMAGES III/MD106-IPHIS cruise (leg II), 1998, Nannofossil biochronology of tephra layers in core MD972143, Benham Rise, western Philippine Sea: Terrestrial, Atmospheric and Oceanic Sciences, v. 9, p. 153–163.

Weimer, P., 1990, Sequence stratigraphy, facies geometries, and depositional history of the Mississippi Fan, Gulf of Mexico: AAPG Bulletin, v. 74, p. 425–453.

Winker, C. D., and J. R. Booth, 2000, Sedimentary dynamics of the salt-dominated continental slope, Gulf of Mexico: Integration of observations from the sea floor, near-surface, and deep subsurface, *in* P. Weimer, R. M. Slatt, J. Coleman, N. C. Rosen, H. Nelson, A. H. Bouma, M. J. Styzen, and D. T. Lawrence, eds., Deep-water reservoirs of the world: Proceedings of the 20th Annual Research Conference, Gulf Coast Section Society for Sedimentary Geology Foundation, p. 1059–1086.

Winn Jr., R. D., H. H. Roberts, B. Kohl, R. H. Fillon, J. A. Crux, A. H. Bouma, and H. W. Spero, 1998, Upper Quaternary strata of the upper continental slope, northeast Gulf of Mexico, sequence stratigraphic model for a terrigenous shelf edge: Journal of Sedimentary Research, v. 68, p. 579–595.

Witrock, R. B., A. R. Friedmann, J. J. Galluzzo, L. D. Nixon, P. J. Post, and K. M. Ross, 2003, Biostratigraphic chart of the Gulf of Mexico offshore region, Jurassic to Quaternary: New Orleans, U.S. Department of the Interior, Minerals Management Service, 1 sheet.